



Open Archive Toulouse Archive Ouverte (OATAO)

OATAO is an open access repository that collects the work of Toulouse researchers and makes it freely available over the web where possible.

This is an author-deposited version published in: <http://oatao.univ-toulouse.fr/>
Eprints ID: 5603

To link to this article: DOI: 10.1007/s11085-011-9241-y
<http://dx.doi.org/10.1007/s11085-011-9241-y>

To cite this version:

Vande Put, Aurélie and Oquab, Djar and Péré, Eve and Raffaitin, Aymeric and Monceau, Daniel *Beneficial Effect of Pt and of Pre-Oxidation on the Oxidation Behaviour of an NiCoCrAlYTa Bond-Coating for Thermal Barrier Coating Systems*. (2011) *Oxidation of Metals*, vol. 75 (n° 5-6). pp. 247-279. ISSN 0030-770X

Any correspondence concerning this service should be sent to the repository administrator: staff-oatao@listes.diff.inp-toulouse.fr

Beneficial Effect of Pt and of Pre-Oxidation on the Oxidation Behaviour of an NiCoCrAlYTa Bond-Coating for Thermal Barrier Coating Systems

Aurélie Vande Put · Djar Oquab · Eve Péré · Aymeric Raffaitin · Daniel Monceau

Abstract The oxidation behaviour of a thermal barrier coating (TBC) system is a major concern as the growth of the thermally grown oxide (TGO) layer on the bond-coating creates stresses that greatly favour the thermal barrier spallation. To delay the loss of the thermal protection provided, research has focused on the bond-coating composition and microstructure as well as on the parameters required for a suitable pre-oxidation treatment before the deposition of the ceramic top coat. Platinum is known to enhance the oxidation/corrosion resistance of MCrAlY coatings. The effect of Pt on the oxidation behaviour of a NiCoCrAlYTa coating was assessed in this study. In addition, pre-oxidation treatments were conducted to determine if the oxidation behaviour of the modified NiCoCrAlYTa coating could be further improved.

Keywords TBC system · Pt · MCrAlY · Oxidation · Pre-oxidation · Bond-coatings

Introduction

Thermal barrier coating systems (TBC systems) are “multi-layered” structures. They are composed of an insulating ceramic top coat (the thermal barrier

A. Vande Put (✉) · D. Oquab · D. Monceau
Institut Carnot CIRIMAT, ENSIACET, 4 allée Emile Monso, BP 44362,
31432 Toulouse Cedex 4, France
e-mail: aurelie.vandeput@ensiacet.fr

E. Péré
Université de Pau et des Pays de l'Adour, IPREM, Hélioparc,
2 Avenue du président d'Angot, 64053 Pau Cedex 9, France

A. Raffaitin
Turbomeca, 64511 Bordes Cedex, France

coating = TBC), an Al-rich metal coating (the bond-coating) and a Ni-base superalloy (the substrate). The top coat is typically made of yttria-stabilized-zirconia (YSZ) and can be deposited by air plasma spray (APS) or electron-beam physical vapour deposition (EB-PVD). Its low thermal conductivity decreases the temperature of the internally cooled underlying substrate. In addition, the columnar microstructure resulting from EB-PVD increases ability of the thermal barrier to accommodate stresses. As YSZ is permeable to oxygen, the bond-coating has to be oxidation resistant. To protect the system against oxidation, the bond-coating is Al-rich in order to form, by reaction with oxygen, a protective, slow growing, adherent and dense thermally grown oxide (TGO) scale of α -Al₂O₃. Because Al₂O₃ is adherent to the bond-coating and to the thermal barrier, the bond-coating also guarantees suitable bonding between the thermal barrier coating and the superalloy.

In service, a TBC system undergoes mechanical and environmental stresses: foreign object damage (FOD) [1, 2], calcium–magnesium–aluminium–silicate (CMAS) deposition [3, 4] or thermomechanical stresses [5]. Environmental stresses lead to thermal barrier coating damage/loss that is detrimental for system lifetime. A key element in the subsequent thermomechanical damage caused to such a system is the formation and growth of the TGO layer between the bond-coating and the thermal barrier. Imperfections in TGO composition, thickness or flatness favour crack initiation and then thermal barrier coating damage. Thus, the bond-coating behaviour under oxidation conditions is very important. Bond-coating oxidation and thus TGO formation start before thermal barrier deposition, during pre-oxidation. This pre-oxidation step is important as various studies have already shown its influence on TBC system lifetime under thermal cycling conditions [6–11].

Three main commercial bond-coating types exist: the β -NiAl aluminide coatings (pure or Pt-modified), the Pt-modified γ -Ni/ γ' -Ni₃Al coatings and the MCrAlY coatings (where M = Ni and/or Co). The β -NiAl coatings and the Pt-modified γ -Ni/ γ' -Ni₃Al coatings are called diffusion coatings when they are formed by the interdiffusion of elements. The MCrAlY coatings are called overlay coatings given that they are made by material deposition.

Because MCrAlY coatings are Cr-rich and alumina-formers, they generally have good resistance against corrosion [12–14]. They also contain the reactive element (RE) yttrium, which is known as being beneficial for TGO adherence [15]. When yttrium content is high with regards to the optimum RE concentration, the TGO layer contains numerous RE-rich oxides that later become pegs. When the peg density is too great, the TBC system lifetime is reduced [8, 16–18]. In terms of oxidation, MCrAlY coatings are not as good alumina-formers as Pt-modified aluminide coatings.

In order to improve the oxidation behaviour of MCrAlY coatings, Pt may be added. This improves oxidation and corrosion resistance [13, 19–25]. As previously mentioned, under oxidation conditions, MCrAlY coatings are known for forming alumina but also other oxides, among them RE-rich oxides. With the addition of Pt, a few studies have shown that the proportion of alumina within the TGO layer is increased. Indeed, a Pt-containing Ni–8Cr–6Al alloy (in wt%) presents, after

oxidation, much less spinels than the corresponding Pt-free alloy [19]. In the studies of Yanar et al. [24] and Quadackers et al. [23], the TGO formed at the interface between the Pt-modified NiCoCrAlY bond-coating and the thermal barrier coating is composed of alumina with no RE-rich oxides. In the work of Quadackers et al. [23], the exact alumina phase(s) was(were) also determined. θ -Al₂O₃ was found with α -Al₂O₃ within TGO, even after an oxidation of 1000 h at 1000 °C. This contrasts with a study of Stott et al. concerning Pt-modified directionally-solidified Ni–Cr–Al–Y–Cr₃C₂ alloys [26]. After 2 h oxidation at 1100 °C in dry oxygen, the oxide layer formed on the Pt-free alloy was mainly composed of θ -Al₂O₃ while a mix of θ -Al₂O₃ and α -Al₂O₃ was observed on the Pt-modified alloy. However, the oxidation temperatures were different in the two studies. The thermal barrier coating present in the work of Quadackers et al. could also be responsible for this difference, as Zhao et al. [27] showed that the top coat delays the transformation of θ -Al₂O₃ into α -Al₂O₃.

With their Al- and Cr-rich composition, MCrAlY coatings offer great resistance against oxidation and corrosion and this is further improved with addition of Pt. To better understand why Pt enhances the oxidation behaviour of the MCrAlY coating, the present study was carried out to compare the behaviour of NiCoCrAlYTa bond-coatings, with and without Pt modification, under isothermal oxidation conditions. Oxidation tests were performed in a thermobalance and the TGO layers formed on the bond-coating surfaces were characterized using XRD, SEM, Raman and fluorescence spectroscopies. The work was completed by assessing pre-oxidation tests to determine if it is possible to enhance even further the oxidation behaviour of the NiCoCrAlYTa-base bond-coatings. Thus, the Pt effect, the superalloy effect, the influence of bond-coating surface preparation and the effect of the oxygen partial pressure on the first oxide were analysed.

Experimental Procedures

Materials Preparation

Systems Without a Thermal Barrier Top Coat

Two nickel-base superalloys were used: AM3, a first-generation superalloy, and MC-NG, a third-generation superalloy that contains rhenium, ruthenium and a small proportion of hafnium. Their compositions are given in Table 1. Both superalloys were machined to give blanks 15 mm × 10 mm × 1 mm with rounded edges. In order to coat the entire surface, a stem made of Hastelloy W or bulk NiCoCrAlYTa was welded to one edge. As they were welded to the superalloy before the bond-coating manufacturing, they became coated in a similar way to the superalloy.

Two bond-coatings were manufactured and deposited on each superalloy: a NiCoCrAlYTa coating and a Pt-modified NiCoCrAlYTa [28]. The 70–80 µm thick NiCoCrAlYTa coating was made by Praxair Surface Technologies (Oldmixon, England) using the Tribomet process. During this process, CrAlYTa particles were

Table 1 Superalloys composition

	Ni	Al	Cr	Co	Ta	Ti	Mo	W	Re	Ru	Hf
AM3											
Mas.%	Bal.	6.0	8.0	6.0	4.0	2.0	2.0	5.0	–	–	–
At.%	Bal.	12.85	8.89	5.88	1.28	2.41	1.2	1.57	–	–	–
MC-NG											
Mas.%	Bal.	6.0	4.0	–	5.0	0.5	1.0	5.0	4.0	4.0	0.1
At.%	Bal.	13.60	4.70	–	1.69	0.64	0.64	1.66	1.31	2.42	0.03

embedded in a growing (Ni, Co) electroplated layer in order to produce uniform dispersion. The Pt-modified NiCoCrAlYTa coating was based on the 70–80 μm thick NiCoCrAlYTa coating (made by the Tribomet process) onto which a $7 \mu\text{m} \pm 2 \mu\text{m}$ Pt-layer was deposited. Irrespective of the type of bond-coating, the specimens were heat treated for 6 h at 1080 °C under secondary vacuum.

Before any surface preparation or oxidation, the stems were cut off creating a non-coated surface (2–7 mm^2). In the case of Hastelloy W stems and when mass measurement was required, the stem stump was polished in order to reduce its length and the un-protected surface given a Sermaloy J coating. Heat treatment under vacuum ensured diffusion bonding of the coating. This step was necessary to improve the oxidation behaviour of the Hastelloy W section. A coating of this type was not necessary with a NiCoCrAlYTa stem.

TBC Systems

Two TBC systems were prepared. They were both composed of the Pt-modified NiCoCrAlYTa coating previously described. One was deposited on AM3 superalloy and the other on MC-NG. The YSZ thermal barrier was then deposited on the bond-coatings after grit blasting the surface (Snecma, Châtelleraut, France). The 150–200 μm thick thermal barrier top coat was deposited by EB-PVD (CCC, Châtelleraut, France).

Hastelloy W stems were also welded to AM3 and to MC-NG superalloys to help in the TBC system processing. Thus, the stems became coated with the bond-coating and the ceramic top coat. Before any oxidation, the Hastelloy W stem was cut off. Unlike the “superalloy + bond-coating” systems, the stem scar was not covered by a Sermaloy J coating, and no thermogravimetric study was therefore possible.

Surface Preparation

Most of the “superalloy + bond-coating” systems were grit blasted before oxidation and pre-oxidation tests. This surface preparation was done at CIRIMAT laboratory (Toulouse, France) using 220 grade corundum, a pressure of around 3 bars and a 45° incidence angle. This was done to remove any oxides which could have formed during heat treatment and to get a uniform surface (at sample scale).

Such grit blasting step is commonly carried out in industry before thermal barrier deposition by EB-PVD. Fresh, unused grit was always used to blast the bond-coating surface to avoid incorporation of impurities on the bond-coating surface, as previously reported by Tolpygo et al. [29].

After grit blasting, the NiCoCrAlYTa stem stubs were ground using ethanol as polishing liquid, in order to reduce the stub length. Before oxidation/pre-oxidation tests, the grit-blasted samples were ultrasonically cleaned in acetone and then in ethanol. Samples were turned over during the cleaning in order to optimise grit blasting residue removal.

When the samples were not grit blasted, cleaning was repeated five times before oxidation and pre-oxidation: acetone, ethanol, water, acetone and ethanol. Water cleaning was necessary to remove salts which would have not been removed by acetone or ethanol. These five steps were not required after grit blasting as the surface was already cleaned from impurities.

Before oxidation, samples with YSZ top coat were rinsed with ethanol once the stem was cut.

Oxidation Testing

Systems Without a Thermal Barrier Top Coat

To study the effect of Pt on the oxidation behaviour of the NiCoCrAlYTa coating, oxidation tests were conducted using a TAG24s thermobalance from SETARAM. Owing to its symmetrical furnace arrangement, the TAG24s thermobalance offers an excellent accuracy (about 1 μg) with limited drift and buoyancy effects. The apparatus records the difference between the mass of the sample and the mass of an inert alumina reference placed in the symmetrical furnace.

Each “superalloy + bond-coating” system that was used to study isothermal oxidation in the thermobalance had a NiCoCrAlYTa stem.

An isothermal oxidation test corresponded to 300 h at 1100 °C under a flow of synthetic air (0.35 l/h). The heating rate was 60 °C/min and the initial cooling rate 90 °C/min (but, overall, 50 min were required to cool from 1100 °C down to room temperature). The mass was re-initialised at zero when the temperature reached 1100 °C.

TBC Systems

The thermal barrier coating systems on AM3 and on MC-NG were also oxidised at 1100 °C for 300 h. They included a cut off Hastelloy W stem whose scar was not covered by a Sermalloy J coating. Mass measurements during oxidation would be distorted by the oxidation of the Hastelloy stem bare surface. So, thermogravimetry analyses were not performed. Instead, the TBC systems were oxidised for 300 h at 1100 °C under laboratory air in a Carbolite muffle furnace. In order to ensure controlled heating, the temperature was increased at a rate of 5 °C/min i.e. much slower than in the thermobalance. After the high temperature dwell, the initial

cooling rate was 20 °C/min. Samples were removed from the furnace once ambient temperature was reached.

Pre-Oxidation Tests

Three pre-oxidation treatments for 1 h at 950 °C were carried out using the TAG24s thermobalance from SETARAM. The same heating and cooling rates as for isothermal oxidation were imposed, i.e. respectively, 60 °C/min and 90 °C/min. Two parameters were studied: the surface preparation and the oxygen partial pressure. The conditions of each pre-oxidation treatment were:

- as-processed surface, primary argon vacuum ($P_{O_2} \approx 4 \times 10^{-4}$ Pa),
- grit-blasted surface, primary argon vacuum ($P_{O_2} \approx 4 \times 10^{-4}$ Pa),
- grit-blasted surface, 0.35 l/h synthetic air flow ($P_{O_2} \approx 2 \times 10^4$ Pa).

After pre-oxidation of grit-blasted surfaces, the specimens were cut in two. One half was kept for oxide characterization. The other was oxidised for 300 h at 1100 °C under laboratory air in a Carbolite muffle furnace in order to study the effect of pre-oxidation on long-term oxidation. The heating and cooling rates were equal to those used during TBC system oxidation (i.e. heating of 5 °C/min and initial cooling of 20 °C/min). The samples were removed from the furnace once ambient temperature was reached.

Summary on Oxidation/Pre-Oxidation Tests

Table 2 summarises the conditions and devices used for each oxidation and pre-oxidation test, as well as the systems.

Materials Characterization

The carbon content of AM3 and MC-NG superalloys was determined by a Carbon & Sulfur analyzer EMIA 920V2 from HORIBA Scientific.

SEM observations of bond-coatings after oxidation and pre-oxidation treatments were performed with a LEO 435VP microscope using the secondary electron imaging mode (SE) or the backscattered imaging mode (BSE). EDS analyses were done with an IMIX system from PGT, in the LEO 435 VP microscope.

X-ray diffraction analyses were done using a Seifert 3000TT apparatus with copper anti-cathode ($\lambda = 1.54056 \text{ \AA}$), with a low angle incidence of 4° or in θ - θ mode.

Raman and fluorescence spectroscopy analyses were made using a T64000 Jobin–Yvon spectrometer equipped with a confocal microscope (whose magnifications are $\times 10$, $\times 50$ or $\times 100$). Spectra were recorded using the 514 nm line of an argon ion laser. The use of a confocal hole of 200 μm gave a 2 μm axial resolution for surface analyses. A CCD detector was used whose spectral field was between 400 nm and 1 μm . Two Raman databases accessible on internet [30, 31] and experimental references were used for spectra identification as well as experimental data on reference materials provided by M. Subanovic from Jülich. Fluorescence

Table 2 Summary of oxidation and pre-oxidation tests

Pre-oxidation		Oxidation		System
Conditions	Apparatus	Conditions	Apparatus	
–	–	300 h at 1100 °C Synthetic air flow	TAG24s	AM3 + NiCoCrAlYTa AM3 + NiCoCrAlYTa-Pt MC-NG + NiCoCrAlYTa-Pt
1 h at 950 °C “as-processed” surface, Argon vacuum	TAG24s	–	–	
1h at 950°C Grit blasted surface, Argon vacuum ^a	TAG24s	300 h at 1100 °C Laboratory air	Muffle furnace	AM3 + NiCoCrAlYTa AM3 + NiCoCrAlYTa-Pt MC-NG + NiCoCrAlYTa MC-NG + NiCoCrAlYTa-Pt
1 h at 950 °C Grit blasted surface, Synthetic air flow ^a				
–	–	300 h at 1100 °C Laboratory air	Muffle furnace	AM3 + NiCoCrAlYTa-Pt + YSZ MC-NG + NiCoCrAlYTa-Pt + YSZ

^a Indicates that after those pre-oxidations, samples were cut in two parts. One half was kept for oxide characterisation, the second half was used for an oxidation for 300 h at 1100 °C

spectroscopy analyses were also performed using the same spectrometer and laser beam.

Results

Samples After Processing

At ambient temperature, the NiCoCrAlYTa coating was composed of β -NiAl and γ -Ni phases [28, 32–36]. The γ' -Ni₃Al phase was present at β -NiAl/ γ -Ni grain boundaries. It was also found within the γ -Ni matrix as fine precipitates probably formed during the cooling part of the heat treatment. Finally, it contained numerous tantalum carbides [28, 34–36]. A small quantity of oxides was also present through the entire depth of the studied coatings [28]. This last observation can be linked to the nature of the MCrAlY coating process, i.e. the electro co-deposition (Tribomet process).

At ambient temperature, the Pt-modified NiCoCrAlYTa bond-coating was like a “dual layer” coating. The outer part of the coating was Pt-rich and composed of L1₀ martensite grains, γ' -Ni₃Al grains and γ -Ni grains with fine γ' -Ni₃Al precipitates. The inner part was composed of the γ -Ni phase that contained small γ' -Ni₃Al precipitates which might have formed during cooling. At high temperature, the L1₀ martensite phase is expected to transform into β -NiAl [28].

More details on the microstructure of those both coatings, and in particular on the effect of Pt addition on the NiCoCrAlYTa coatings, can be found in the Vande Put et al. study [28]. The “superalloy + bond-coating” systems used for

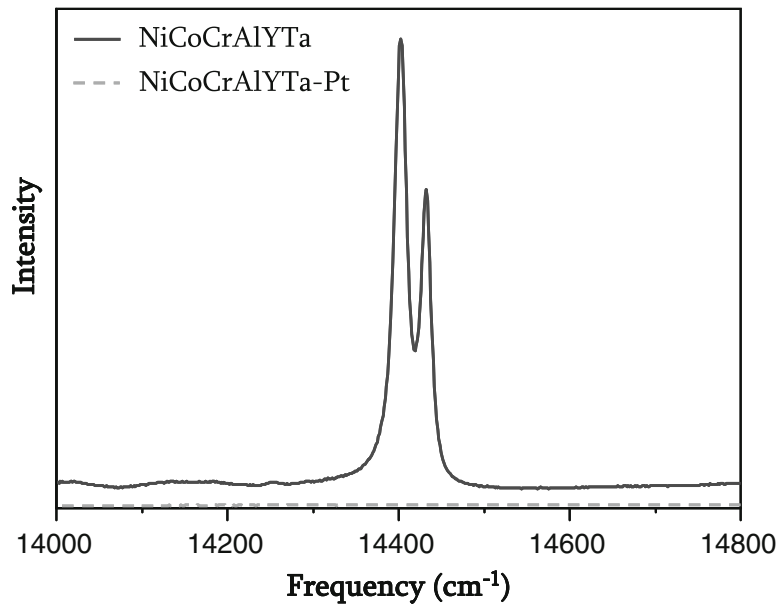


Fig. 1 Fluorescence spectroscopy on bond-coating surface after heat treatment (AM3 superalloy)

the present study came from the same batch as the systems characterized in [28]. The differences in the unmodified and Pt-modified NiCoCrAlYTa microstructures were explained as resulting from the strong Al transport from the coating core to the Pt-rich surface. This transport was linked to the decrease in Al activity due to Pt addition, already demonstrated by other authors in other systems [37–39].

After processing, the as-processed surfaces of each bond-coating were analysed by fluorescence spectroscopy (Fig. 1). The spectrum obtained for the NiCoCrAlYTa coating (continuous line) corresponded to Cr^{3+} fluorescence spectrum from $\alpha\text{-Al}_2\text{O}_3$. The dotted line spectrum was obtained with the Pt-modified NiCoCrAlYTa coating. On another hand, no band relative to $\alpha\text{-Al}_2\text{O}_3$ or transient Al_2O_3 appeared in the spectrum of Pt-modified NiCoCrAlYTa coating (dotted line). This suggests that this bond-coating was not or was very little oxidized after heat treatment under secondary vacuum at 1080 °C.

The Raman spectrum of Pt-free NiCoCrAlYTa, between 600 and 1800 cm^{-1} (Fig. 2), showed the presence of YAlO_3 .

Oxidation Testing

TGA Analysis: Determination of the Oxidation Kinetics

Three “superalloy + bond-coating” systems were oxidized for 300 h at 1100 °C under synthetic air flow in a thermobalance (Table 2). The mass gains during the high temperature dwells are plotted in Fig. 3. It is clear that mass gains were much lower when Pt was added. In the case of the Pt-modified NiCoCrAlYTa coating, mass gains appeared to be lower with MC-NG superalloy than with AM3 superalloy.

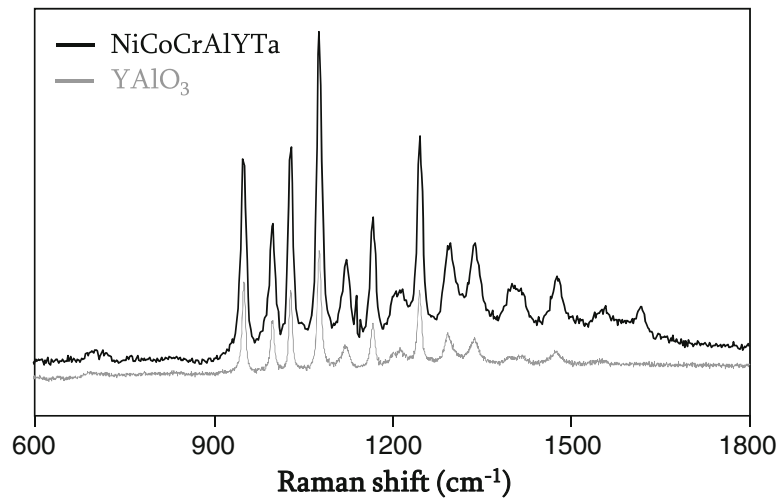


Fig. 2 Raman spectrum obtained on NiCoCrAlYTa surface after heat treatment. YAlO₃ reference

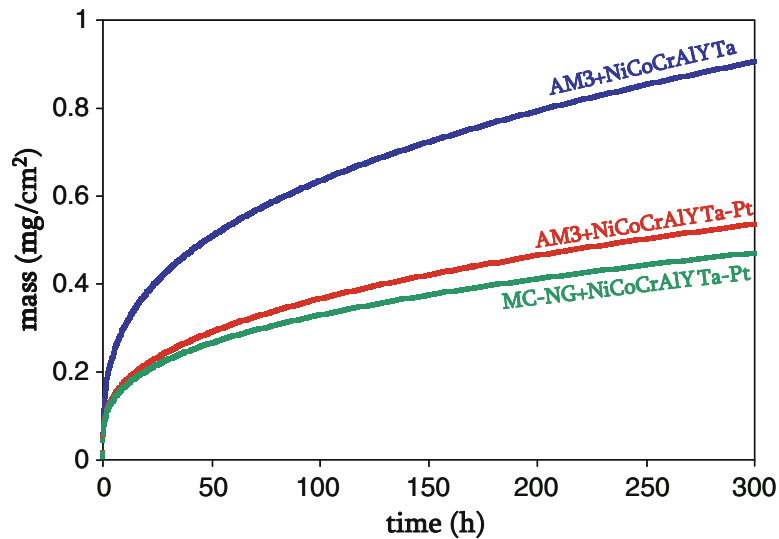


Fig. 3 Mass gain of the systems during the oxidation test at 1100 °C under flowing synthetic air

Using these mass gains, the oxidation rate constants k_p were calculated using a complete parabolic law fitting procedure [40]. The values obtained, calculated for different time intervals, are summarised in Table 3. We also plotted k_p versus time during the first hours of oxidation (Fig. 4). For the NiCoCrAlYTa-base system, the oxidation rate constant of the transient oxidation stage (0–1 h) was similar to that of a single crystal of polished nickel aluminide (with a low sulphur content) determined in a study of Cadoret et al. ($3.6 \times 10^{-6} \text{ mg}^2 \text{ cm}^{-4} \text{ s}^{-1}$) [41]. In the quasi-steady-state stage, the oxidation rate constant became closer to that of a β -NiAl alloy forming α -Al₂O₃ (Fig. 5) [42]. Compared to MCrAlY-based systems, the k_p values obtained were lower than those of a “CMSX-2 + NiCoCrAlYTa” system oxidised under O₂ at 1100 °C [33]. In this last study, the NiCoCrAlYTa coating was deposited by low pressure plasma spraying and did not receive

Table 3 Parabolic rate constant k_p measured for different time intervals, oxidation at 1100 °C under synthetic air flow

Time interval (h)	k_p ($\text{mg}^2 \text{cm}^{-4} \text{s}^{-1}$)			
	0–1	1–300	100–300	200–300
AM3 + NiCoCrAlYTa	3.7×10^{-6}	3.8×10^{-7}	2.8×10^{-7}	2.7×10^{-7}
AM3 + NiCoCrAlYTa-Pt	1.0×10^{-6}	1.5×10^{-7}	1.5×10^{-7}	1.1×10^{-7}
MC-NG + NiCoCrAlYTa-Pt	1.1×10^{-6}	1.0×10^{-7}	8.6×10^{-8}	7.7×10^{-8}

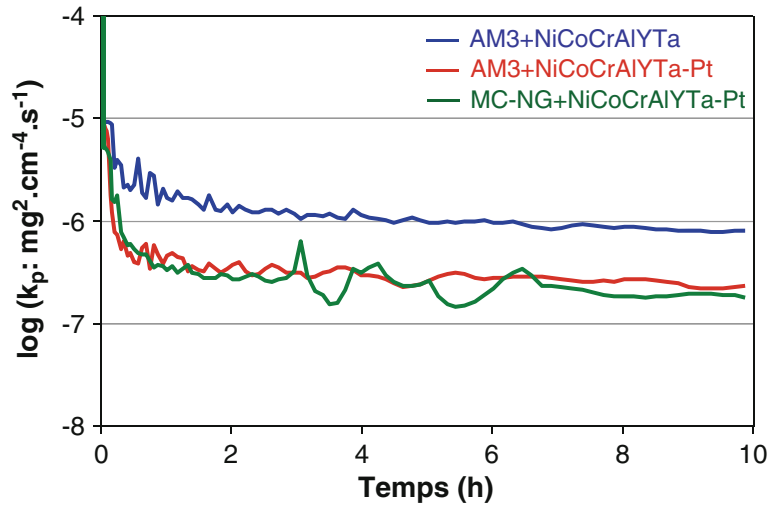


Fig. 4 k_p versus time during the oxidation at 1100 °C under flowing synthetic air

any surface preparation. The k_p was calculated in that case to be equal to $1.5 \times 10^{-6} \text{ mg}^2 \text{cm}^{-4} \text{s}^{-1}$ between 5 and 100 h. The values reported in Table 3 for the “AM3 + NiCoCrAlYTa” system were also lower than those of a bulk NiCoCrAlYTa oxidised at 1100 °C under O_2 [34]. This material was manufactured using the “Tribomet” process and polished before the oxidation test. The k_p , calculated over 500 h of oxidation, was equal to $7.2 \times 10^{-7} \text{ mg}^2 \text{cm}^{-4} \text{s}^{-1}$.

With the addition of Pt, the oxidation rate constant decreased by a factor of 2–2.5 (Table 3). According to Table 3 and Fig. 4, the effect of Pt on oxidation kinetics started from the first hour of oxidation and the superalloy effect appeared after a few hours of oxidation. During the transient oxidation stage (0–1 h), the oxidation rate constant of the systems comprising a Pt-modified NiCoCrAlYTa coating was lower than that of a single crystal of polished Pt-modified nickel aluminide ($7.8 \times 10^{-6} \text{ mg}^2 \text{cm}^{-4} \text{s}^{-1}$) [41]. During the quasi-steady-state oxidation stage, the oxidation rate constant was a little lower than that of a β -NiAl alloy that forms α - Al_2O_3 (Fig. 5) [42]. The values were slightly higher with AM3 superalloy and slightly lower with MC-NG superalloy than those of a Pt-modified aluminised sample of NiCoCrAlYTa made by spark plasma sintering and oxidised at 1100 °C. The k_p for that last system was equal to $9 \times 10^{-8} \text{ mg}^2 \text{cm}^{-4} \text{s}^{-1}$ when calculated for the first 192 h [43].

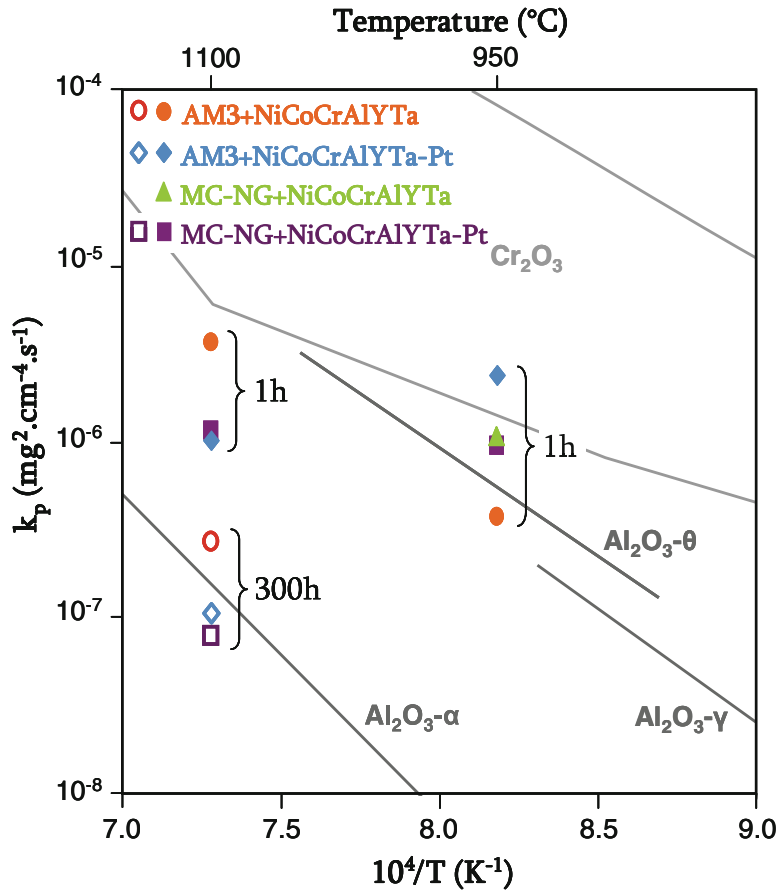


Fig. 5 Arrhenius graph. k_p are calculated from the high temperature dwells of the pre-oxidation under synthetic air at 950 °C and the oxidation at 1100 °C without pre-oxidation (between 0 and 1 h or 200 and 300 h). γ -, θ - and α - Al_2O_3 lines are from [42], Cr_2O_3 domain from [75]

Oxide Identification

The TGO layers developed during isothermal oxidation were identified by XRD analysis in low incidence configuration. The XRD spectra are presented in Fig. 6. On top of Fig. 6 is the spectrum corresponding to the “AM3 + NiCoCrAlYTa” system. For 300 h at 1100 °C under synthetic air, various oxides formed on the NiCoCrAlYTa coating whose external part was composed of γ -Ni. The most intense peaks were attributed to α - Al_2O_3 while the others corresponded to NiAl_2O_4 , YTao_4 , AlTaO_4 , TiTaO_4 and $\text{Y}_3\text{Al}_5\text{O}_{12}$. Alumina was the main oxide, but fast growing oxides also composed the TGO layer. In contrast, α - Al_2O_3 was the only oxide detected at the surface of the Pt-modified NiCoCrAlYTa coatings, except a small peak attributed to NiAl_2O_4 , after 300 h at 1100 °C under synthetic air for both superalloy substrates (Fig. 6). After oxidation, the Pt-modified NiCoCrAlYTa sub-surface was composed of γ -Ni and γ' - Ni_3Al phases.

To locally analyse the TGO layers formed, Raman spectroscopy was done on the TGO layer after 300 h at 1100 °C under synthetic air. The Raman spectra of the oxidised NiCoCrAlYTa coating presented many bands which could be attributed to a mixture of Al-Y-rich oxides, but precise identification was difficult due to the complexity of the spectra. By contrast, the Raman spectra of oxidised Pt-modified

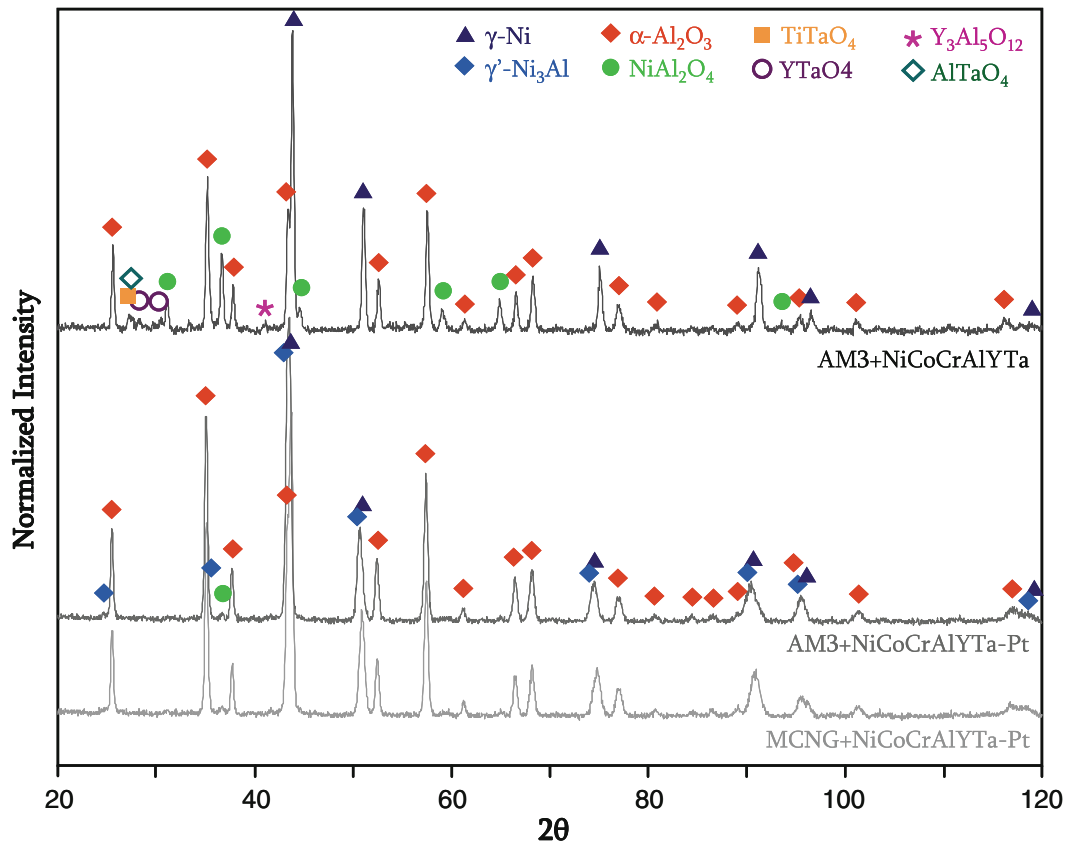
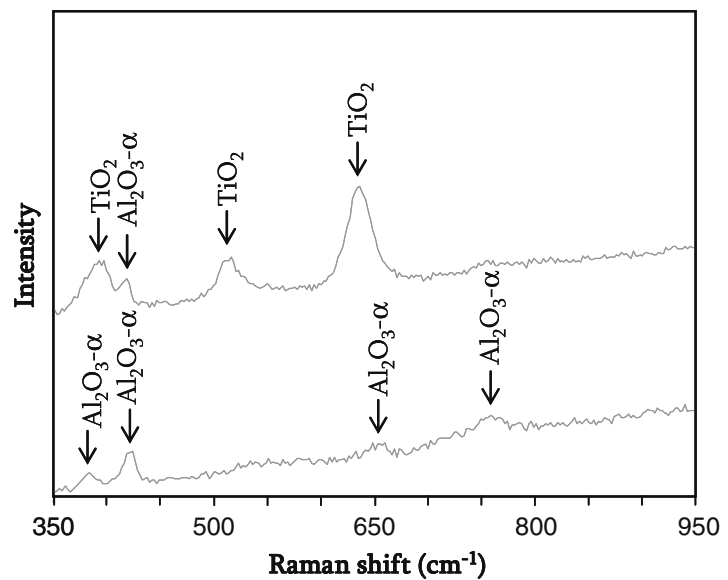


Fig. 6 XRD analysis on bond-coating surfaces after oxidation for 300 h at 1100 °C under synthetic air

Fig. 7 Raman spectra obtained on NiCoCrAlYTa-Pt after oxidation (AM3 superalloy)



NiCoCrAlYTa coatings revealed a few bands attributed to α - Al_2O_3 . When the Pt-modified NiCoCrAlYTa coating was deposited on AM3 superalloy and depending on the analysed zone, TiO_2 -anatase bands appeared in addition to α - Al_2O_3 (Fig. 7). No TiO_2 bands were obtained when the Pt-modified NiCoCrAlYTa coating was deposited on MC-NG superalloy.

Despite the fact that only α -Al₂O₃ with a very small proportion of NiAl₂O₄ were detected by XRD, some particles were visible with the SEM on the TGO surface of Pt-modified NiCoCrAlYTa bond-coating. According to EDS analyses, these precipitates were rich in refractory elements and calcium.

Pt Effect on TGO Adherence

Owing to the precise mass measurements of the thermobalance, the net mass changes during the high temperature dwell of 300 h at 1100 °C could be compared to the total mass changes during the oxidation treatment which included heating and cooling in addition to the high temperature dwell. The data are given in Table 4.

With the NiCoCrAlYTa coated system, the total mass gain was much lower than that determined during the high temperature dwell. This is because the stresses generated during cooling led to TGO spallation.

For Pt-modified NiCoCrAlYTa coatings, the total mass gains were greater than those measured during the high-temperature dwell. Such a difference is due to the oxidation that occurred during heating (oxidation and spallation during cooling being negligible in this case).

The oxide scale spallation from the NiCoCrAlYTa coating was confirmed by SEM observation of the oxidised surface (Fig. 8). On these SEM images made in the BSE mode, the oxide appeared dark while the bond-coating presented a light, shiny contrast. It was obvious that oxide spallation occurred with the NiCoCrAlYTa bond-coating whereas the TGO layer was well adherent to the Pt-modified NiCoCrAlYTa bond-coating. Only light spallation was noted on the Pt-modified NiCoCrAlYTa coating deposited on MC-NG superalloy, mainly on sample edges. The specific geometry of edges may favour spallation; however, such mass loss is not evident in Table 4. The oxidation being under synthetic air of high purity, water vapour could also have favoured oxide scale spallation on furnace opening [44, 45]. Another possibility is that the mass gain during heating was greater than mass loss due to spallation on cooling.

Isothermal Oxidation of TBC Systems

After 300 h at 1100 °C under laboratory air, the TBC systems exhibited a small fraction of TBC spallation (Fig. 9). Figure 9a and b show the two faces of the TBC on the AM3-base system while Fig. 9c and d are the two faces of the TBC on the MC-NG-base system. The proportion of spalled TBC was larger with the AM3 superalloy substrate.

Table 4 Mass gains during isothermal oxidation for 300 h at 1100 °C, determined using the TAG24s thermobalance

	$\Delta m/S$ during the high temperature dwell at 1100 °C (mg cm ⁻²)	Total $\Delta m/S$ (mg cm ⁻²)
AM3 + NiCoCrAlYTa	0.90	0.71
AM3 + NiCoCrAlYTa-Pt	0.53	0.58
MC-NG + NiCoCrAlYTa-Pt	0.47	0.51

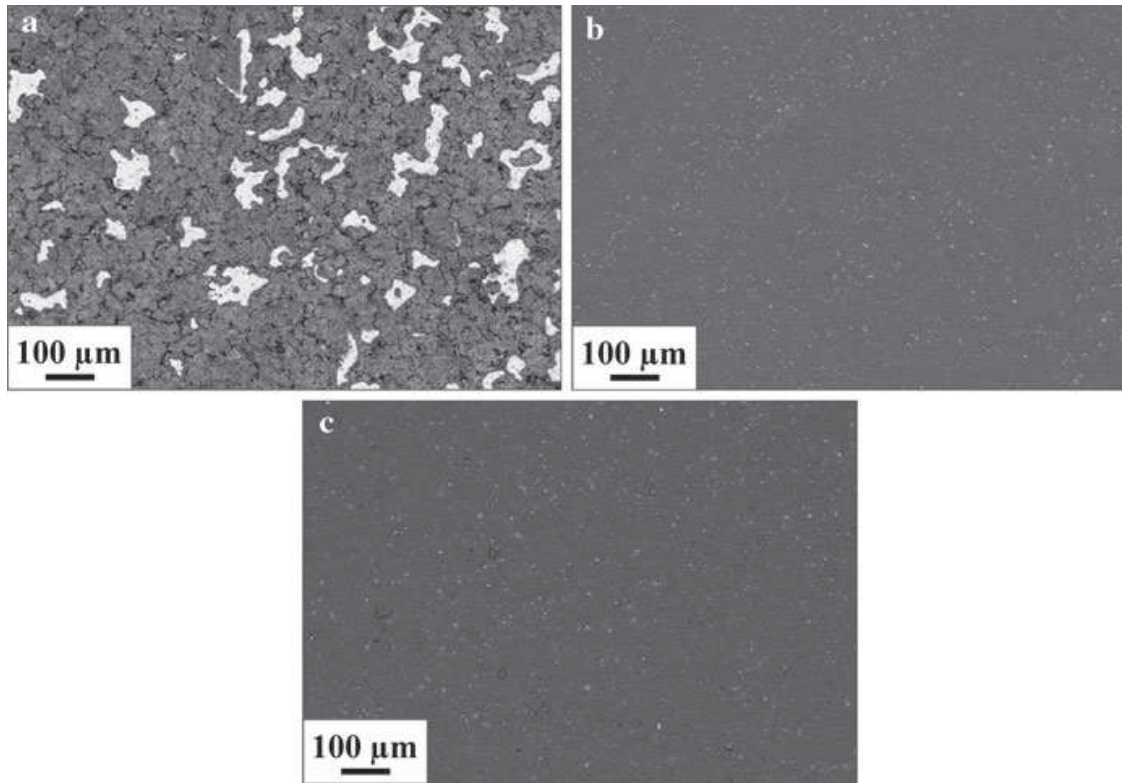


Fig. 8 Oxide scales after oxidation on **a** NiCoCrAlYTa bond-coating on AM3, **b** Pt-modified NiCoCrAlYTa bond-coating on AM3, **c** Pt-modified NiCoCrAlYTa bond-coating on MC-NG. SEM images in BSE mode

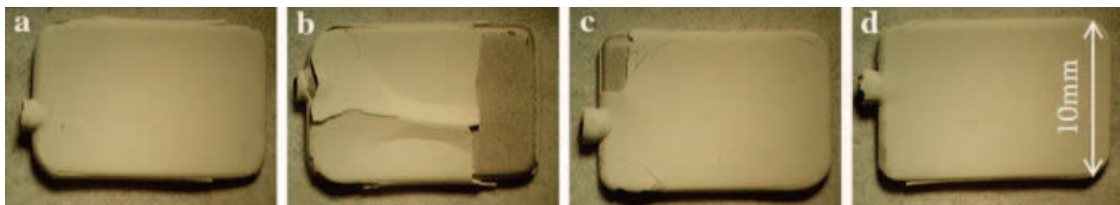


Fig. 9 TBC systems after 300 h at 1100 °C under laboratory air. **a–b** AM3 superalloy, **c–d** MC-NG superalloy

Figure 10 shows SEM cross-sections of TBC systems focusing on the TGO layer. The thermal barrier coating was still adherent to the TGO which itself was detached from the bond-coating. No oxide other than alumina was found within the TGO using EDS. The external surface of the TGO could not be analysed by EDS as the thermal barrier coating did not separate from TGO. Therefore, it was not possible to check for the presence or absence of titanium oxide at the TGO external surface.

It was shown in a previous publication [28] that the outer surface of the Pt-modified NiCoCrAlYTa coating was initially composed of L1₀ martensite grains and γ' -Ni₃Al grains as well as γ -Ni grains containing fine γ' -Ni₃Al precipitates. The inner zone of the coating was composed of the γ -Ni phase that presented fine γ' -Ni₃Al precipitates. Tantalum carbides were found within the bond-coating, close to the interface with the superalloy. They were dispersed through a larger thickness when the superalloy was MC-NG compared to AM3. After 300 h of oxidation at

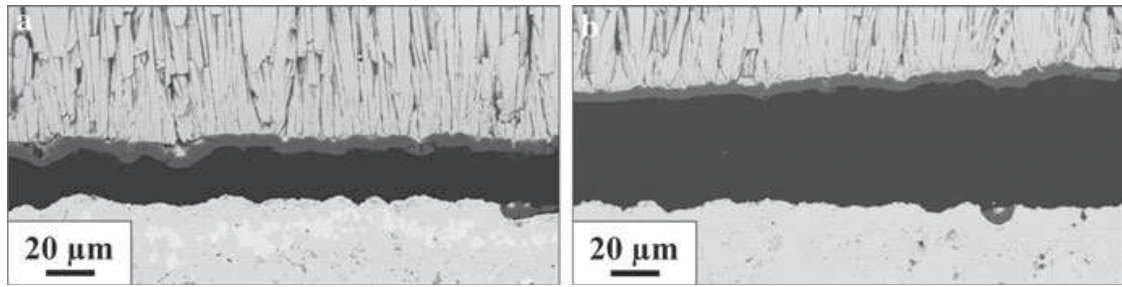


Fig. 10 TBC system cross-sections after 300 h at 1100 °C under laboratory air. **a** AM3 superalloy, **b** MC-NG superalloy. SEM images in BSE mode

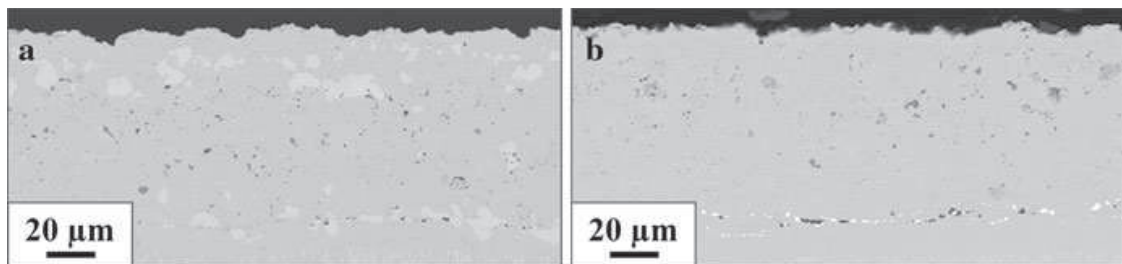


Fig. 11 Cross-sections of Pt-modified NiCoCrAlYTa bond-coatings of the TBC systems oxidised 300 h at 1100 °C under laboratory air. SEM images in BSE mode. γ' -Ni₃Al phase has the brightest contrast compared to γ -Ni

1100 °C, Al consumption to form the TGO layer, Pt diffusion towards the superalloy and the diffusion of elements from the superalloy towards to the coating led to a microstructure mainly composed of γ -Ni (Fig. 11) with the sub-surface of the Pt-modified NiCoCrAlYTa coating on AM3 including some γ' -Ni₃Al (Fig. 11a). In addition, tantalum carbides completely dissolved during oxidation. In the case of the Pt-modified NiCoCrAlYTa coating on MC-NG, the bond-coating was entirely γ -Ni but tantalum carbides were still observed (Fig. 11b). Nevertheless, their volume fraction was much reduced as they were only located at the interface with the superalloy.

Pre-Oxidation Study

TGA Analysis: k_p Determination

For each pre-oxidation treatment, the mass changes during the total oxidation test were recorded (total $\Delta m/S$ from TGA). Samples were also weighed before the introduction within the thermobalance and after their removal from the thermobalance (total $\Delta m/S$ from weighings) (Tables 5, 6). In the case of both pre-oxidation treatments under vacuum, mass gains at 950 °C were so small that the vacuum pumping disturbed the mass recording (note that a mass change of 0.0185 mg/cm² corresponds to an alumina scale of 100 nm thick). Therefore, the net mass change curves could not be used to calculate a parabolic rate constant. When pre-oxidation was performed under synthetic air, the mass gains during the high-temperature

Table 5 Net mass changes during the pre-oxidation treatments under vacuum

	“as-processed” surface, argon vacuum		Grit blasted surface, argon vacuum	
	Total $\Delta m/S$ from TGA (mg cm^{-2})	Total $\Delta m/S$ from weighings (mg cm^{-2})	Total $\Delta m/S$ from TGA (mg cm^{-2})	Total $\Delta m/S$ from weighings (mg cm^{-2})
AM3 + NiCoCrAlYTa	0.027	0.018	0.029	0.023
AM3 + NiCoCrAlYTa-Pt	-0.073	-0.096	0.015	0.018
MC-NG + NiCoCrAlYTa	0.037	0.029	0.031	0.027
MC-NG + NiCoCrAlYTa-Pt	0.014	0.003	N.A.	N.A.

N.A. non-available

Table 6 Net mass changes and k_p measured for the pre-oxidation under synthetic air

	Grit blasted surface, Synthetic air flow			
	$\Delta m/S$ during the dwell at 950 °C from TGA (mg cm^{-2})	Total $\Delta m/S$ from TGA (mg cm^{-2})	Total $\Delta m/S$ from weighings (mg cm^{-2})	k_p^a ($\text{mg}^2 \text{cm}^{-4} \text{s}^{-1}$)
AM3 + NiCoCrAlYTa	0.037	0.053	0.046	3.8×10^{-7}
AM3 + NiCoCrAlYTa-Pt	0.090	0.147	0.104	2.4×10^{-6}
MC-NG + NiCoCrAlYTa	0.068	0.098	0.111	1.0×10^{-6}
MC-NG + NiCoCrAlYTa-Pt	0.060	Error	0.084	9.5×10^{-7}

^a k_p calculated from 0 to 3600 s

dwell ($\Delta m/S$ during the dwell at 950 °C from TAG) were larger and allowed acceptable determination of the oxidation kinetic constants (Table 6). The k_p values were calculated during the high temperature dwell at 950 °C using a complete parabolic law fitting procedure [40].

Despite the difficulty of the measurements for the pre-oxidations under vacuum, it was still possible to observe that the mass gains measured for the NiCoCrAlYTa-base systems were larger than those of the Pt-modified NiCoCrAlYTa-base systems. No difference was observed between an as-processed surface and a grit-blasted surface (Table 5).

The different trends in mass changes observed for pre-oxidation under vacuum between the unmodified and Pt-modified NiCoCrAlYTa-base systems were not observed with the pre-oxidation under synthetic air. In the case of synthetic air, the oxidation rates were similar for the various systems, except for the “AM3 + NiCoCrAlYTa” system, which exhibited a lower oxidation rate (Table 6).

Oxide Characterization After Pre-Oxidation

After pre-oxidation treatment, oxide scales were analysed using fluorescence and Raman spectroscopies. The TGO composition identified for each system after the

Table 7 Oxide scale characterisation on NiCoCrAlYTa coating on AM3 substrate

AM3	Fluorescence		Raman		
Ar vacuum, «as-processed» surface					
Without Pt	α -Al ₂ O ₃	–	YAlO ₃	Cr ₂ O ₃	Y ₃ Al ₅ O ₁₂ ?
With Pt	α -Al ₂ O ₃	–	–	–	–
Ar vacuum, Grit blasted surface					
Without Pt	α -Al ₂ O ₃	θ -Al ₂ O ₃	YAlO ₃	Cr ₂ O ₃	Y ₃ Al ₅ O ₁₂ ?
With Pt	α -Al ₂ O ₃	–	–	–	–
Synthetic air, Grit blasted surface					
Without Pt	α -Al ₂ O ₃	θ -Al ₂ O ₃	YAlO ₃	Cr ₂ O ₃	–
With Pt	α -Al ₂ O ₃	θ -Al ₂ O ₃	–	–	–

Table 8 Oxide scale characterisation on NiCoCrAlYTa coatings on MC-NG substrate

MC-NG	Fluorescence		Raman		
Ar vacuum, «as-processed» surface					
Without Pt	α -Al ₂ O ₃	–	YAlO ₃	Cr ₂ O ₃	–
With Pt	α -Al ₂ O ₃	–	–	–	–
Ar vacuum, Grit blasted surface					
Without Pt	α -Al ₂ O ₃	(θ -Al ₂ O ₃)	YAlO ₃	Cr ₂ O ₃	–
With Pt	α -Al ₂ O ₃	–	–	–	–
Synthetic air, Grit blasted surface					
Without Pt	α -Al ₂ O ₃	θ -Al ₂ O ₃	YAlO ₃	Cr ₂ O ₃	Y ₃ Al ₅ O ₁₂ ?
With Pt	α -Al ₂ O ₃	θ -Al ₂ O ₃	–	–	–

The brackets mean that the alumina peak is very small

three pre-oxidation treatments is summarized in Tables 7 and 8, corresponding respectively to systems based on the AM3 superalloy substrate and the MC-NG superalloy substrate. The brackets around θ -Al₂O₃ in these tables indicate that the peak corresponding to this oxide is very small.

The first observation was that whatever the pre-oxidation treatment, alumina, chromia and mixed oxides were identified within the TGO formed on the NiCoCrAlYTa bond-coating; whereas, only alumina was detected on the Pt-modified NiCoCrAlYTa coating.

Concerning the alumina formed during pre-oxidation, it differed regarding the pre-oxidation treatment and the bond-coating. Irrespective of the bond-coating and the superalloy, α -Al₂O₃ was the only alumina detected after pre-oxidation under vacuum on an as-processed surface. After a pre-oxidation under vacuum on a grit-blasted surface, a small fraction of θ -Al₂O₃ was detected in addition to α -Al₂O₃ for NiCoCrAlYTa-base systems. Only α -Al₂O₃ was found on the grit-blasted surface of Pt-modified NiCoCrAlYTa-base systems after pre-oxidation under vacuum. With the increase in oxygen partial pressure, θ -Al₂O₃ and α -Al₂O₃ were both identified on grit-blasted surfaces of each system. Nevertheless, the fraction of α -Al₂O₃ was much larger than that of θ -Al₂O₃.

Oxide Morphology After Pre-Oxidation

Figure 12 presents the morphology of the TGO layer formed during the different pre-oxidation treatments on the Pt-modified NiCoCrAlYTa coating deposited on AM3. On an as-processed surface, the pre-oxidation under vacuum led to a very fine microstructure that changed with the bond-coating grain orientation (Fig. 12b). Many oxide grains looked elongated (needles).

With a grit-blast surface finish, tiny needles reminiscent of transient alumina morphology were visible after pre-oxidation under vacuum (Fig. 12c). Nevertheless, the amount of these needles was greatly reduced compared to an as-processed surface (Fig. 12a, b).

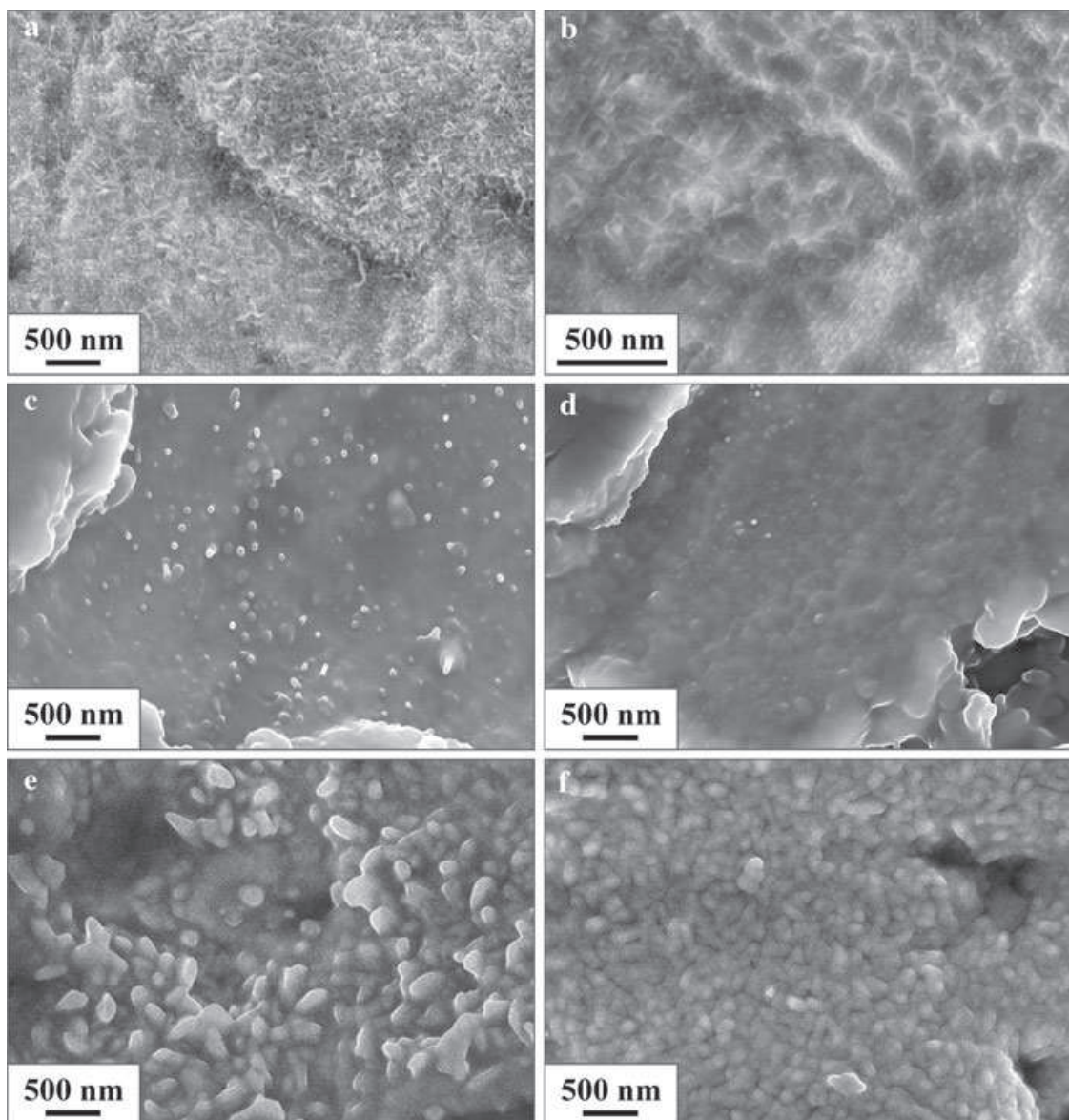


Fig. 12 Pt-modified NiCoCrAlYTa bond-coating on AM3 after pre-oxidation. **a** and **b** as-processed surface, pre-oxidation under vacuum. **c** and **d** grit blasted surface, pre-oxidation under vacuum. **e** and **f** grit blasted surface, pre-oxidation under synthetic air. **e** Concave region which probably was lightly or no grit blasted

After pre-oxidation under synthetic air of a grit-blasted surface, the oxide grains were larger than after a pre-oxidation under vacuum (Fig. 12f). In zones that were less accessible to the grit blasting, small platelets were visible (Fig. 12e).

Similar oxide scale morphologies were observed after pre-oxidation of the Pt-modified NiCoCrAlYTa coating on the MC-NG superalloy (Fig. 13).

Effect of Pre-Oxidation on Subsequent Oxidation Behaviour of Pt-NiCoCrAlYTa Bond-Coatings

In order to study the influence of pre-oxidation on the oxidation behaviour of both bond-coatings, the samples that were grit blasted before the pre-oxidation were oxidised for 300 h at 1100 °C under laboratory air. Although all the TGO layers formed on NiCoCrAlYTa-coated systems partially spalled after these “pre-oxidation + oxidation” sequences, no spallation was observed with the Pt-modified NiCoCrAlYTa bond-coating, irrespective of the superalloy.

Although there was no difference in spallation resistance with Pt-modified NiCoCrAlYTa bond-coatings, the oxide morphology differed depending on the oxygen partial pressure used for the pre-oxidation (Fig. 14). When the pre-oxidation was carried out under vacuum, few platelets or needles were visible at the TGO surface, despite the long isothermal oxidation for 300 h at 1100 °C under laboratory air (Fig. 14a–d). Such platelets and whiskers were not observed at the TGO surface after 300 h at 1100 °C following pre-oxidation under synthetic air (Fig. 14e–h).

In Fig. 15, TGO morphology after 300 h at 1100 °C following pre-oxidation under air at 950 °C is compared to TGO morphology after 300 h at 1100 °C without any pre-oxidation, on a MC-NG superalloy. Despite a similar heating rate between pre-oxidation and oxidation, oxide grains at the TGO surface looked equiaxial when pre-oxidation was performed (Fig. 15a); whereas, oxide grains appeared elongated at the TGO surface without pre-oxidation (Fig. 15b). Fairly similar morphology variations were observed with AM3 superalloy, but surface contamination made meaningful observations difficult.

The morphology of elongated oxide grains was specific to the TGO surface, as shown in the TGO fracture presented in Fig. 16. Indeed, it can be seen that the oxide scales were duplex, with an external sub-layer formed of small equiaxial crystallites and an internal sub-layer with larger columnar grains. This microstructure was typical of inward growing α -Al₂O₃ scales [46].

Discussion

Effect of Pt on Oxidation

TGA analyses performed on the three “superalloy + bond-coating” systems highlighted the decrease in oxidation kinetics by Pt addition (Figs. 3, 4, 5, Table 3). As seen in Fig. 5, Pt-modified NiCoCrAlYTa coatings formed a continuous α -Al₂O₃ layer. In the case of NiAl single crystals, it was shown that Pt slows down the transformation from transient alumina to α -Al₂O₃ and therefore

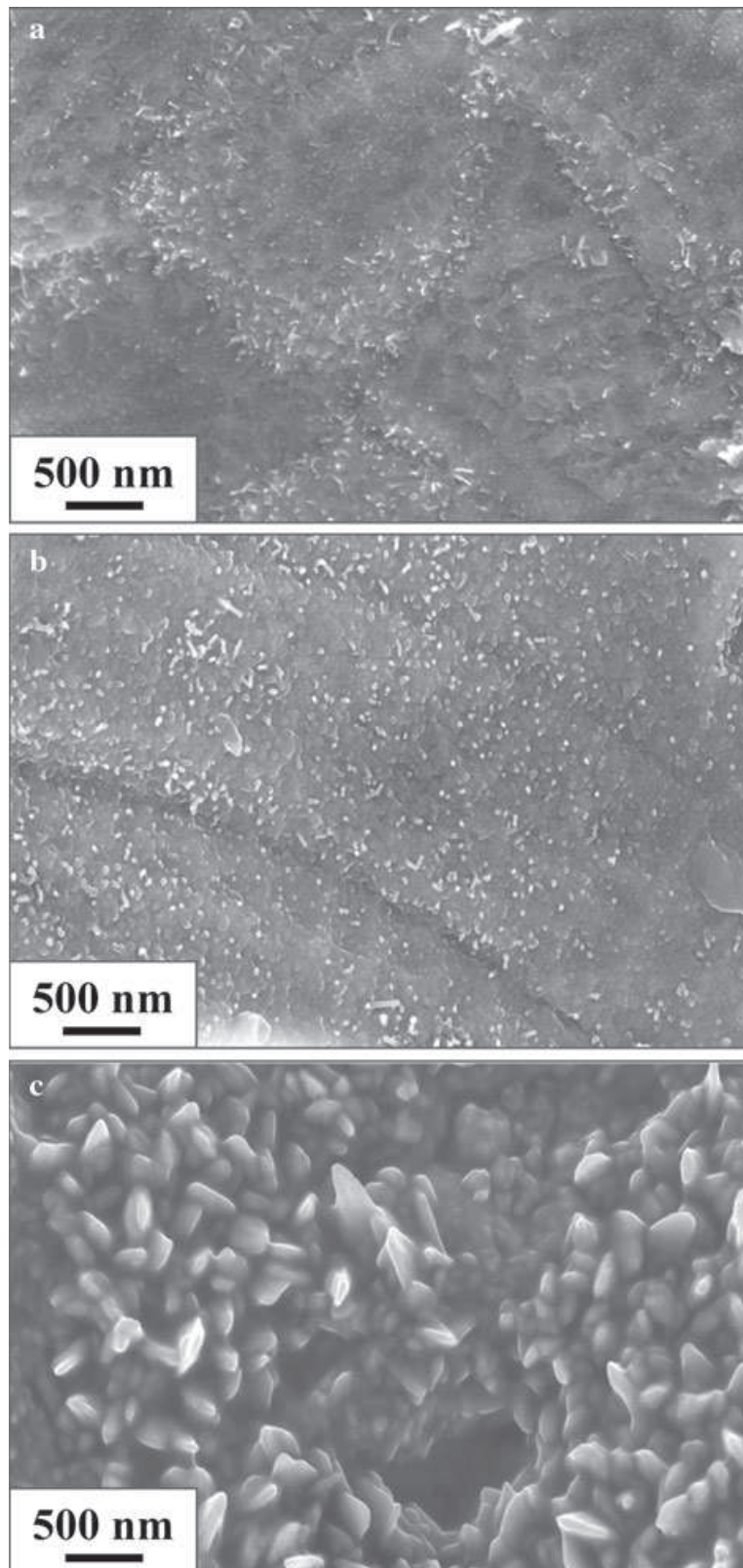


Fig. 13 Pt-modified NiCoCrAlYTa bond-coating on MC-NG after pre-oxidation. **a** As-processed surface, pre-oxidation under vacuum. **b** Grit blasted surface, pre-oxidation under vacuum. **c** Grit blasted surface, pre-oxidation under synthetic air

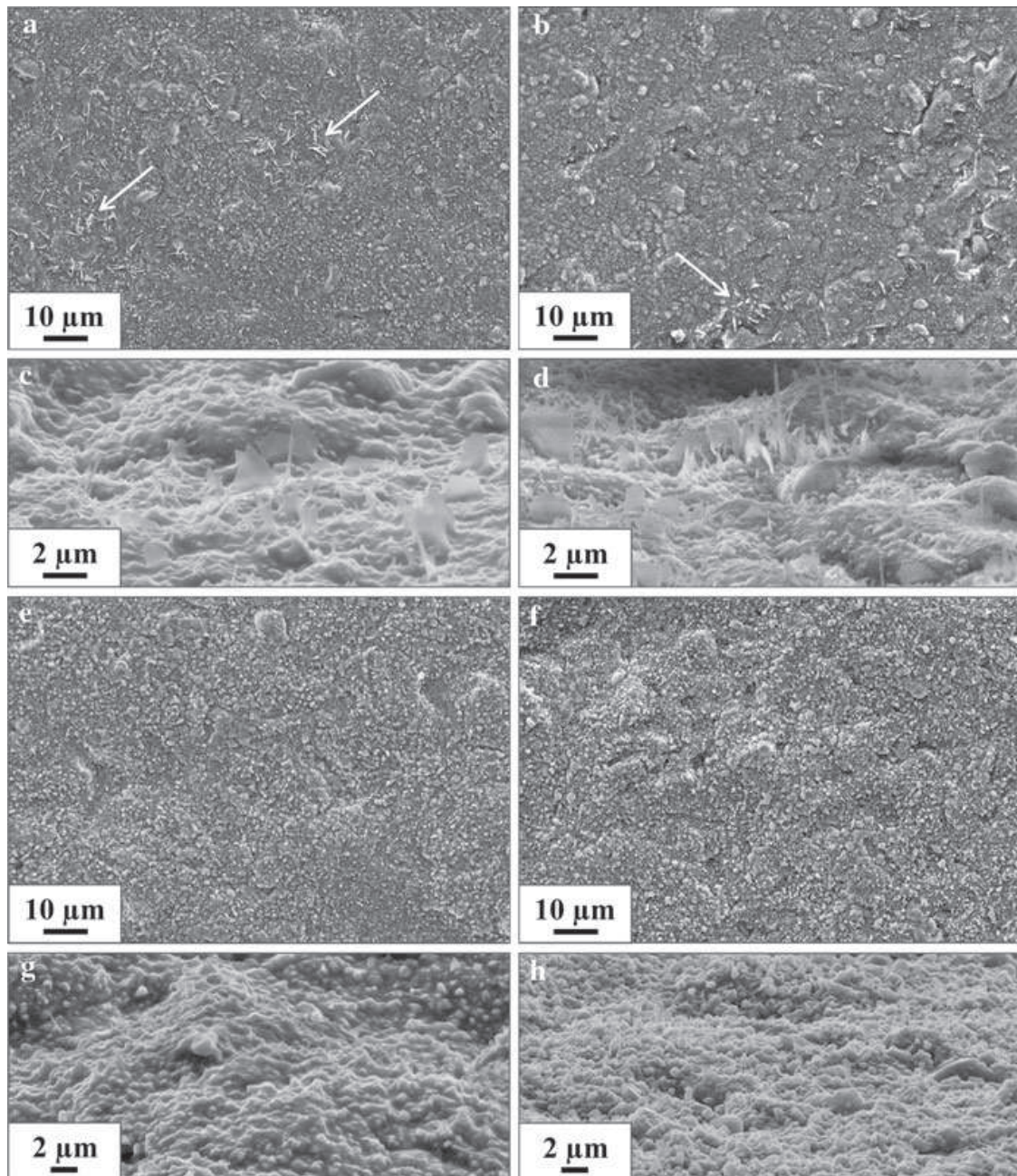


Fig. 14 Oxide scale formed on NiCoCrAlYTa-Pt coating deposited on **a, c, e, g** AM3; **b, d, f, h** MC-NG, after pre-oxidation and oxidation for 300 h at 1100 °C. **a–d** Grit blasted surface, pre-oxidation under vacuum, **e–h** grit blasted surface, pre-oxidation under synthetic air. *White arrows* indicate whiskers/platelets

increases oxidation kinetics [41]. In the present study, only a small proportion of θ -Al₂O₃ was found by photoluminescence spectroscopy after 1 h at 950 °C under synthetic air irrespective of the bond-coating material. After the pre-oxidation under vacuum, only α -Al₂O₃ was detected at the surface of the Pt-modified NiCoCrAlYTa coatings; whereas, a small peak of θ -Al₂O₃ appeared on the photoluminescence spectrum of the NiCoCrAlYTa bond-coating in addition to α -Al₂O₃ peaks. Thus, and in contrast to the previous study on NiAl, this indicated that the addition of Pt did not favour transient alumina formation. This could be due to the presence of Cr

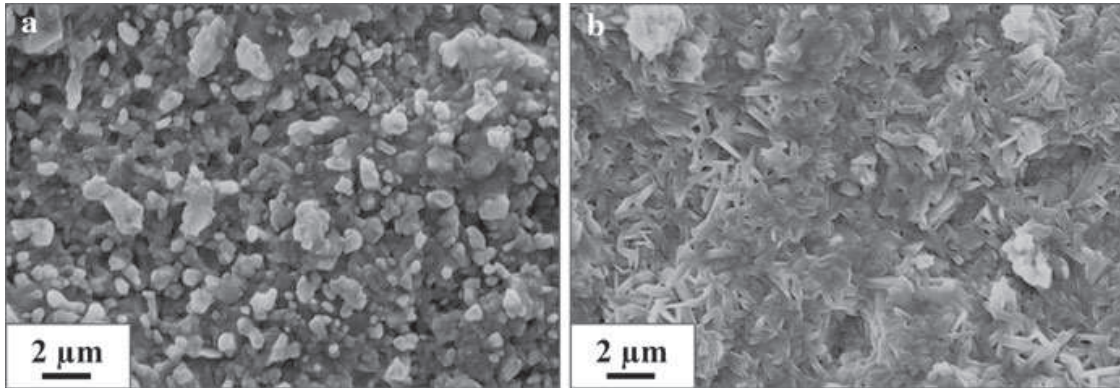


Fig. 15 Oxide scale morphology formed during the oxidation of 300 h at 1100 °C on grit blasted Pt-modified NiCoCrAlYTa on MC-NG superalloy. **a** Pre-oxidation under synthetic air, **b** without any pre-oxidation

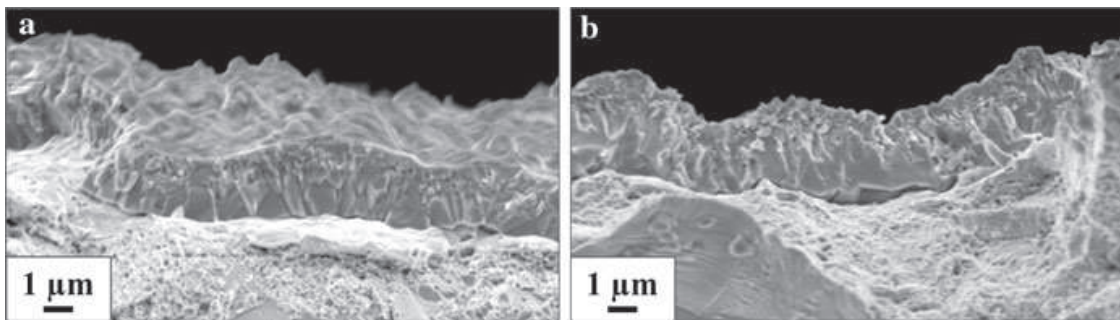


Fig. 16 Fracture of TGO layer formed on Pt-modified NiCoCrAlYTa bond-coating after 300 h at 1100 °C under flowing synthetic air in thermobalance **a** AM3 superalloy, **b** MC-NG superalloy

in the NiCoCrAlYTa coating as Cr is known to favour α -Al₂O₃ nucleation [42]. A reduced fraction of transient alumina could explain a decrease in the oxidation kinetics. However, the oxidation rate constants calculated from the mass changes during the high-temperature dwell of the pre-oxidation of 1 h at 950 °C under synthetic air were close in the various systems, except for the “AM3 + NiCoCrAlYTa” system which had slower oxidation kinetics than the three other systems. This difference between that system and the others could be explained by the fact that this sample came from an older batch of specimens. The “Tribomet” process could have changed slightly leading to NiCoCrAlYTa coatings with slightly different characteristics. The small proportion of transient alumina remaining after the pre-oxidation treatment under synthetic air and the small effect of Pt on the pre-oxidation kinetics showed that the explanation for the slower oxidation kinetics at 1100 °C for 300 h with Pt does not involve transient alumina. The proposed explanation is in fact much simpler. While α -Al₂O₃ and various faster-growing oxides were detected at the surface of the NiCoCrAlYTa coating after 300 h at 1100 °C (Fig. 6), only α -Al₂O₃ with a small fraction of NiAl₂O₄ were identified on oxidised Pt-modified NiCoCrAlYTa bond-coatings. With addition of Pt, the sub-surface of the Pt-modified NiCoCrAlYTa coating became enriched in Al after the heat treatment compared to a simple NiCoCrAlYTa coating [28]. This large

increase in the Al content of the external part of the Pt-modified NiCoCrAlYTa coating, leading to the formation of a β -phase outer layer, favoured the selective oxidation of aluminium. As fewer fast growing oxides were formed, the oxidation kinetics were slowed.

In addition to the Pt effect, the superalloy substrate seems to affect the oxidation kinetics (Figs. 3, 4, 5 and Tables 3, 4). MC-NG is a third generation superalloy that contains hafnium. Hafnium is a reactive element like yttrium. Reactive elements are known for improving the oxidation behaviour of materials. Among the various effects of reactive elements, one is the decrease in the oxidation kinetics [15, 47]. Then, the hafnium contained within MC-NG superalloy could diffuse towards the alumina (as shown by [48]) and segregate at alumina grain boundaries. As hafnium was present within the superalloy and not within the original bond-coating like yttrium, it took some time to see its effect on mass gain during oxidation. The beneficial effect of co-doping with RE elements is in agreement with previous works on different materials [49, 50].

Titanium oxide was also detected within the TGO layer but only on the “AM3 + NiCoCrAlYTa-Pt” system (Fig. 7). This means that titanium diffused from the superalloy through the bond-coating and oxidised at the surface. Titanium diffusion through a MCrAlY coating and its oxidation was observed by Tawancy et al. [51] and Hesnawi et al. [52]. Vialas et al. observed, after processing, Ti + Ta-rich particles at the surface of an inward grown Pt-modified aluminide coating on CMSX-4 superalloy, but not on IN792 or SCB superalloys [53]. But these coatings were high-activity Pt-modified aluminides, that are usually believed to be more sensitive to superalloy composition than MCrAlY coatings. This last point can be questioned because many elements have a higher solubility in γ -phase than in β -phase. In this study, although numerous zones were analysed on each Pt-modified NiCoCrAlYTa coating (deposited on AM3 and MC-NG), TiO₂ was only detected within TGO with superalloy AM3. This discrepancy is likely due to the difference in composition between AM3 and MC-NG. AM3 and MC-NG superalloys have a titanium concentration equal to 2.4 and 0.6 at.%, respectively. Indeed, in TBC coated Pt-modified superalloys, Tawancy et al. reported that the larger the titanium concentration, the greater the occurrence of spallation [51]. Therefore, this difference in titanium concentration could be responsible for the absence of TiO₂ when MC-NG was the substrate. The possible influence of the superalloy composition on the absence/presence of TiO₂ after oxidation supports a superalloy effect on the oxidation behaviour of a Pt-modified NiCoCrAlYTa coating.

Some authors have reported a beneficial effect of low titanium contents on oxidation behaviour, but a damaging effect when titanium is at high concentrations [54, 55]. Most authors, however, agree that titanium is harmful with regards to oxidation [32, 33, 51–53, 56–58]. In order to prevent the harmful effect of titanium, tantalum was added to the NiCoCrAlY coatings. Tantalum traps the titanium and carbon that diffuse from the superalloy towards the TGO [12, 22, 59, 60] by forming (Ta,Ti)C carbides within the bond-coating [12, 59]. Then, the titanium can no longer diffuse towards the TGO. The tantalum decreases the superalloy effect on oxidation behaviour [32]. As previously mentioned, Pt-modified NiCoCrAlYTa coatings contained tantalum carbides. Located close to the interface with the superalloy, the

zone affected by tantalum carbides was thicker with MC-NG substrate than with AM3 superalloy [28]. Carbon, present within the superalloy, could also influence carbide formation. In the present work, the carbon contents in AM3 and MC-NG superalloys were measured. A concentration of 31.7 ppm (wt) was obtained for AM3 while a content of 16.8 ppm (wt) was obtained for MG-NG. Therefore, the difference in carbon concentration could not be responsible for the carbide proportion. Besides, using the diffusion data for carbon in γ -Ni ($D = 0.11 \cdot \exp(-139000/RT)$ cm²/s [61]) it can be calculated that carbon diffuses fast enough to go through the entire coating thickness during diffusion heat treatment (6 h at 1080 °C) to form carbides.

After 300 h at 1100 °C, no more tantalum carbides were observed within the Pt-modified NiCoCrAlYTaN on AM3 and only few were observed at the MC-NG/Pt-modified NiCoCrAlYTaN coating interface. During oxidation, aluminium was consumed at the bond-coating/TGO interface to form the oxide layer. Chemical elements also diffused from the bond-coating to the superalloy (such as Pt, Al) and from the superalloy towards the bond-coating (such as Ti, Ni). A previous study on Pt-modified NiCoCrAlYTaN bond-coatings, coming from the same batch as the ones of the present work, showed that MC-NG-base systems were fabricated with a thinner Pt layer than the AM3-base systems [28]. It was proposed that the difference in this initial Pt thickness layer was responsible for the larger carbide volume fraction for MC-NG-base systems. Indeed, the idea was put forward that Pt could decrease tantalum activity and therefore destabilise tantalum carbides [28]. The fact that the tantalum carbide volume fraction was greatly decreased or even became nil after 300 h at 1100 °C (i.e. after Pt diffusion) supports this hypothesis. Based on the EDS spectral maps from [28], the average Pt concentration corresponding to the limit between the carbide-free zone and the carbide-rich zone within the Pt-modified NiCoCrAlYTaN bond-coating could be determined after heat treatment. It was equal to respectively, 1.2 and 2.2 at.% with AM3 and MC-NG superalloys. After 300 h of oxidation at 1100 °C, the Pt concentration was also determined. This was done by an EDS analysis on one or two zones and not by EDS spectral maps. The Pt concentration just above the interface between the bond-coating and the superalloy was 4.0 at.% with AM3 and 2.5 at.% with MC-NG. So, if the Pt concentrations previously determined for the bond-coating after heat treatment are the limit concentration for tantalum carbide precipitation, it could be expected to observe complete dissolution of the carbides with AM3 superalloy. With MC-NG, the complete dissolution of carbides within the bond-coating is consistent with the limit in Pt concentration. Nevertheless, many carbides were still present at the bond-coating/superalloy interface. This could be due to the higher Ta concentration of MC-NG superalloy compared to AM3 superalloy (1.7 at.% for MC-NG against 1.3 at.% for AM3) which could lead to Ta diffusion from the superalloy towards the bond-coating.

With regard to titanium, the reduction in carbide volume fraction within the bond-coatings could also explain titanium diffusion towards TGO as it was no longer trapped within carbides. Therefore, the absence of TiO₂ at the surface of the Pt-modified NiCoCrAlYTaN on MC-NG would not be due to titanium concentration in the superalloy but rather be the result of a lower quantity of Pt deposited on the

NiCoCrAlYTa surface (see [28] for more details). It is important to note that in the present study, the TGO layer was detached from the bond-coating but still well adherent to the YSZ thermal barrier. TiO₂ did not lead to TGO spallation, but the oxidation time was short (300 h) and the amount of TiO₂ was low. The presence of TiO₂ at the TGO/thermal barrier interface could later be detrimental, due to stress development. More work has to be done to fully elucidate the effect of titanium diffusion through the TGO.

After the same oxidation for 300 h at 1100 °C, the “AM3 + NiCoCrAlYTa” system underwent spallation while the systems composed of a Pt-modified NiCoCrAlYTa coating did not. So, Pt apparently improved TGO adherence to the bond-coating. The difference in spallation resistance could be explained by a chemical effect of platinum on TGO adherence. Pt could improve TGO adherence by trapping sulphur, but yttrium concentration is high within the bond-coating so it is difficult to rationalise that Pt could improve sulphur trapping even more. Pt could also favour TGO adherence by enhancing θ -Al₂O₃ formation which would lead to lower stresses at the end of the complete transformation into α -Al₂O₃ [41, 53]. However, the TGO characterization performed after the various pre-oxidation treatments did not reveal such an effect of Pt with these coatings. Another point is that the metallic phases present within the bond-coating sub-surface differed with/without Pt. L1₀ martensite grains, γ' -Ni₃Al grains and γ -Ni grains composed the external part of the Pt-modified NiCoCrAlYTa coating whereas β -NiAl, γ' -Ni₃Al and γ -Ni phases composed the entire NiCoCrAlYTa coating. With the increase in temperature, the martensite transforms to β -NiAl. The volume change associated with this transformation is 2.0% ± 0.3% [62, 63]. In Pt-modified aluminide coatings, this volume change can favour bond-coating surface rumpling [64] as well as β -NiAl to γ' -Ni₃Al transformation [65]. A previous study showed that without Pt, NiCoCrAlYTa-base TBC systems do not rumple whereas Pt-modified nickel aluminide coating-base TBC systems do [66]. Thus, it is well established that L1₀ martensite is harmful for the TBC system lifetime. Nevertheless, the martensite-containing Pt-modified MCrAlY was superior to the MCrAlY coating in the present study. This can be explained by the fact that because of the presence of the L1₀ martensite phase (β -NiAl phase at high temperature) in the outer part of the coating due to the increase in aluminium concentration, there was less yttrium, tantalum and titanium in the external part of the coating, see [28]. This favoured exclusive alumina formation, as well as the presence of chromium within the external layer (Cr-rich γ -Ni grains were mixed with martensite grains). With Pt addition, the TGO was mainly composed of alumina; whereas, fast-growing oxides and yttrium-rich oxides also formed on NiCoCrAlYTa bond-coatings. Fast-growing oxides and yttrium-rich oxides favoured stress development due to different coefficients of thermal expansion. They also created heterogeneities in TGO thickness and composition which also led to stress concentration. These stresses degraded the TGO which spalled earlier.

During the oxidation (300 h at 1100 °C), the TBC systems microstructure evolved due to elements diffusion (to form the TGO layer and between the bond-coating and the superalloy). After the test, the bond-coating deposited on AM3 was mainly composed of the γ -Ni phase with the sub-surface including some γ' -Ni₃Al

while the bond-coating deposited on MC-NG was only composed of the γ -Ni phase, with few carbides at the bond-coating/superalloy interface. The presence of γ' -Ni₃Al grains in the case of the AM3-base TBC system is not in agreement with the higher oxidation rate constant of the “AM3 + Pt-modified NiCoCrAlYTa” system compared to the “MC-NG + Pt-modified NiCoCrAlYTa” system. The oxidation kinetics being greater, more Al should be consumed and therefore the Al-rich phases should disappear faster. However, the AM3-base systems had a larger Pt quantity than the MC-NG-base systems. As explained previously, the Pt-rich sub-surface led to an Al diffusion from the coating bulk towards the surface. As more Pt was added for the AM3-base systems, the Al diffusion was expected to be greater below the surface and to remain high for a longer time. The presence of γ' -Ni₃Al grains only with the AM3 substrate despite a higher oxidation kinetics than the MC-NG-base system highlights the strong effect of Pt on Al diffusion.

Pre-Oxidation Study and Pt Effect

The mass gains resulting from both pre-oxidations under vacuum were extremely low, suggesting that the oxide scale formed was very thin especially with a Pt-modified NiCoCrAlYTa coating (Table 5). The total mass gains measured by weighings are in agreement with the trend of the total mass gains recorded by the thermobalance. The systems with a Pt-modified NiCoCrAlYTa bond-coating showed lower mass gains compared to unmodified NiCoCrAlYTa systems, whether the surface was as-processed or grit blasted. The TGO layer that formed on the Pt-modified NiCoCrAlYTa bond-coatings was only composed of α -Al₂O₃, whereas alumina, chromia and Y, Al-rich oxides were identified on the NiCoCrAlYTa bond-coatings after pre-oxidation under vacuum. The decrease in mass gains observed for the Pt-modified bond-coating can be explained by the increase in aluminium concentration below the bond-coating surface (as in the case of oxidation for 300 h at 1100 °C).

When the NiCoCrAlYTa bond-coating was grit blasted, θ -Al₂O₃ was detected after pre-oxidation under vacuum whereas only α -Al₂O₃ was identified on the as-processed surface (Tables 7, 8). Grit blasting is known to favour α -Al₂O₃ formation [7, 67, 68], which is in apparent opposition to what was observed here. An important point to remember is that the as-processed NiCoCrAlYTa surface was already oxidised after the diffusion heat treatment (α -Al₂O₃ and YAlO₃ were detected, Figs. 1, 2). In contrast, the as-processed Pt-modified NiCoCrAlYTa surface was not (or was very lightly) oxidised. When a continuous and sufficiently thick α -Al₂O₃ layer was present at the surface of a material, the growth of θ -Al₂O₃ stopped and θ -Al₂O₃ transformed into α -Al₂O₃. When no grit blasting was performed, this thin oxide layer remained on the NiCoCrAlYTa surface before the pre-oxidation. Despite the presence of YAlO₃ within the TGO (oxygen diffuses faster in YAlO₃ than in α -Al₂O₃), this α -Al₂O₃ layer ensured an effective barrier against oxidation and so lower mass gains were obtained. With the addition of Pt, things differed. Only α -Al₂O₃ was identified by fluorescence spectroscopy on both surfaces (as-processed/grit blasted) after pre-oxidation under vacuum. Nevertheless, the morphology of the oxide layer formed on the as-processed surface recalled

transient alumina. On the grit-blasted surface, a few tiny whiskers characteristic of transient alumina were observed. Even though no θ -Al₂O₃ bands appeared, θ -Al₂O₃ could have formed and completely transformed to α -Al₂O₃ before the end of the pre-oxidation. The remains of the θ -Al₂O₃ morphology were observed but only α -Al₂O₃ was detected.

Regarding the oxide morphology, the grit blasting step homogenised the surface state and consequently the morphology of the TGO layer (Fig. 12a–d).

With the increase in oxygen partial pressure during the pre-oxidation treatment, θ -Al₂O₃ formation was apparently favoured. It was difficult to determine how the fraction of transient alumina changed with the oxygen partial pressure as the fluorescence response of θ -Al₂O₃ is much lower than that of α -Al₂O₃. With the increase in oxygen partial pressure, the TGO morphology evolved slightly towards platelets rather than needles. Such morphology, typical of transient alumina/oxide, was mainly observed in regions that were not accessible to grit blasting. This confirms the effect of grit blasting favouring α -Al₂O₃ formation.

Concerning the possible effect of the superalloy on the beginning of oxidation, no difference was noted with the present results.

It was shown by Cadoret et al. [41] that Pt slows down the θ -Al₂O₃ \rightarrow α -Al₂O₃ transformation and therefore increases the oxidation kinetics of single crystal NiAl. In the present work, the experiments carried out do not allow a conclusion on the effect of Pt on the kinetics of the θ -Al₂O₃ \rightarrow α -Al₂O₃ transformation. According to the fluorescence spectroscopy results, Pt did not favour θ -Al₂O₃ formation. This is in agreement with the study of Stott et al. [26] who found less transient alumina after oxidation of a Pt-containing Ni–Cr–Al–Y–Cr₃C₂ alloy compared to the corresponding Pt-free alloy. But these results are in opposition with Quadackers et al. [23] who detected θ -Al₂O₃ within the TGO of Pt-modified NiCoCrAlY based TBC systems after 1000 h at 1000 °C. However, in [23] the surface preparation before thermal barrier deposition by EB-PVD was not mentioned and the oxidation was carried out at a relatively low temperature. Our observation that Pt did not favour θ -Al₂O₃ formation is also in contradiction with the study of Stiger et al. [69] where a continuous mixed zone was observed in TBC systems composed of a Pt-modified NiCoCrAlYTaN bond-coating (a mixed zone is considered by many authors as being the result of the presence of transient alumina before thermal barrier deposition [69–73]). Nevertheless, the thermal barrier could have had an influence on θ -Al₂O₃ formation as Zhao et al. inferred that the YSZ thermal barrier delayed the θ -Al₂O₃ \rightarrow α -Al₂O₃ transformation [27].

In the present work, Pt did not have a strong influence on the type of alumina formed during pre-oxidation. At the surface of the NiCoCrAlYTaN coating, there were β -NiAl grains and Cr-rich γ -Ni. Grains of L1₀ martensite coexisted with grains of γ -Ni and γ' -Ni₃Al phases which were Cr-rich. Like grit blasting, chromium is known to favour α -Al₂O₃ nucleation on β -NiAl [42]. The high Cr concentration in the external part of both bond-coatings could have mitigated the Pt effect. It would be interesting to carry out the same study on the oxidation of systems with a Pt-modified NiCoCrAlYTaN bond-coating composed of a NiCoCrAlYTaN deposited by vacuum plasma spraying. As explained in a previous study, the processing route used to deposit the NiCoCrAlYTaN greatly influences the bond-coating

microstructure after the diffusion heat treatment [28]. Contrary to the present Pt-modified NiCoCrAlYTaNi bond-coating (obtained by the “Tribomet” process), a Pt-modified coating comprising a vacuum plasma sprayed NiCoCrAlYTaNi coating is composed of a continuous outer layer of martensite (with some γ' -Ni₃Al grains). In this layer, the chromium concentration is much lower than the chromium concentration within the external zone of the present Pt-modified NiCoCrAlYTaNi. The Cr concentration being lower, the effect of the oxidation/pre-oxidation could be more significant, as α -Al₂O₃ nucleation would probably not be so enhanced. This last point is important given that it could explain why transient alumina was observed in the studies of Quadackers et al. [23] and Stiger et al. [69].

Effect of Pre-Oxidation on the Following Oxidation for Pt-Modified NiCoCrAlYTaNi Bond-Coatings

As spalling occurred in all the TGO layers formed on the systems containing a NiCoCrAlYTaNi bond-coating after 300 h at 1100 °C following a pre-oxidation, we focussed on the Pt-modified NiCoCrAlYTaNi systems. For these systems, the TGO layer remained adherent to the bond-coating after pre-oxidation and oxidation for 300 h at 1100 °C. Despite no difference being observed on spallation resistance, the TGO morphology changed slightly with the oxygen partial pressure established during the pre-oxidation (all the systems studied here were grit blasted before pre-oxidation). Whereas θ -Al₂O₃ was detected after pre-oxidation under synthetic air, no needles/platelets were observed after the following oxidation of 300 h. In contrast, no θ -Al₂O₃ was detected after pre-oxidation under vacuum but after the following oxidation of 300 h needles and platelets were observed, recalling transient alumina/oxide.

As previously mentioned, as soon as a continuous and sufficiently thick layer of α -Al₂O₃ is present at the surface of a material, the growth of θ -Al₂O₃ stops and it transforms into α -Al₂O₃. Therefore, it was surprising to observe needles and platelets after 300 h of oxidation at 1100 °C, the temperature at which transient alumina rapidly transforms into α -Al₂O₃. Transient alumina could form at crack location during the slow cooling at the end of the oxidation but no cracks were visible. In a study conducted by Matsumoto et al., it is recommended not to carry out pre-oxidation under a too low oxygen partial pressure before the thermal barrier deposition if the aim is to form a continuous α -Al₂O₃ layer [11]. In the case of their study, the bond-coating was a polished CoNiCrAlY and they estimated the limit in oxygen partial pressure to be around 10⁻¹² Pa. In the present study, we were far from such a vacuum ($P_{O_2} = 10^{-4}$ Pa here). Nevertheless, after the diffusion heat treatment of 6 h at 1080 °C under secondary vacuum, no alumina was detected by fluorescence spectroscopy on the Pt-modified NiCoCrAlYTaNi surface. This suggests that the bond-coating was not or only very lightly oxidised and therefore that a sufficient oxygen partial pressure is required to form a continuous alumina layer. Secondly, the total mass gains measured in the thermobalance during the pre-oxidation under vacuum were extremely low suggesting that the oxide layer formed after this treatment was very thin. In order to reach the oxidation temperature of 1100 °C, slow heating was done (5 °C/min) under laboratory air. This slow heating

favoured transient alumina growth [74]. A possible explanation could be that when pre-oxidation was carried out under synthetic air, θ -Al₂O₃ and α -Al₂O₃ formed and remained until the end of the pre-oxidation. As the pre-oxidation was carried out under a high oxygen partial pressure, α -Al₂O₃ formed a layer thick enough to stop θ -Al₂O₃ growth that rapidly transformed into α -Al₂O₃ during the slow heating to 1100 °C. When pre-oxidation was performed under vacuum, θ -Al₂O₃ and α -Al₂O₃ both formed (according to TGO morphology) but θ -Al₂O₃ rapidly became transformed into α -Al₂O₃ as such oxygen partial pressure prevented transient alumina formation. α -Al₂O₃ was the only oxide remaining at the end of the pre-oxidation, but was not continuous or thick enough to prevent θ -Al₂O₃ under higher oxygen partial pressure. During the slow heating to 1100 °C, θ -Al₂O₃ could grow. It rapidly transformed into α -Al₂O₃ when the high temperature dwell was reached. Nevertheless, this hypothesis does not explain why whiskers and platelets were maintained for such a long time at 1100 °C.

Regarding the oxidation treatments studied (300 h at 1100 °C), the oxygen partial pressure of the pre-oxidation did not influence the resistance to oxide scale spallation. This is for systems without a thermal barrier coating for which the presence of whiskers or/and platelets on top of the TGO layer is not harmful in terms of spallation resistance. In TBC systems, the bond-coating could behave differently in terms of oxidation. The first oxide that forms could differ from what is observed here. A few results and studies support this last point. First, the thickness of the TGO layers which formed on the systems without a thermal barrier coating oxidised for 300 h at 1100 °C, was 3.2 μ m with the AM3 superalloy and 2.8 μ m with the MC-NG superalloy. This is much thinner than the TGO layers observed on the TBC system cross-sections after 300 h at 1100 °C, which were about 4.5–5 μ m thick regarding the superalloy (Fig. 10). Concerning the TBC systems, the pre-oxidation which was carried out was the regular industrial pre-oxidation included in the EB-PVD process. Knowing that the presence of the thermal barrier delayed the θ -Al₂O₃ \rightarrow α -Al₂O₃ transformation [27], if a small proportion of transient alumina was present at the bond-coating surface before EB-PVD, a mixed zone probably formed. Besides, θ -Al₂O₃ probably did not completely transform into α -Al₂O₃ before the end of the pre-oxidation. With the slow heating of the oxidation at 1100 °C and the presence of the thermal barrier coating, the transient alumina was maintained for a longer time than without the TBC. As θ -Al₂O₃ grows 10–100 times faster than α -Al₂O₃, the TGO became thicker. Stiger et al. [74] reported also an important difference in TGO thickness between the bond-coating with and without the top coat. They attributed the thicker TGO in the presence of the TBC to the formation of a mixed zone composed of an alumina matrix containing YSZ particles. In the literature, the formation of the mixed zone is associated to the presence of transient alumina before thermal barrier deposition [69–73]. So, both these arguments take into account the presence of transient alumina at the bond-coating surface after the pre-oxidation. The pre-oxidation step usually carried out in industry is performed in such a way that α -Al₂O₃ is the main oxide present within TGO before the deposition of the thermal barrier. Considering this last point, it would be surprising to get a thicker TGO in industrial TBC systems. Besides, no mixed zone was visible using SEM which supports the fact that no transient alumina

was present before thermal barrier deposition. The surface preparation on the bond-coating surface could also lead to different TGO thickness after oxidation. Grit blasting has been shown to favour α -Al₂O₃ formation [7, 67, 68]. According to Tolpygo et al. [29], the grit blasting brings impurities on the bond-coating surface which are then incorporated into the alumina layer leading to a high oxidation rate and a lower resistance to spallation. In the present study, the bond-coating without the TBC and the bond-coating with the TBC were grit blasted before oxidation/thermal barrier deposition. Nevertheless, the grit blasting was not performed in the same place. The systems without the TBC were grit blasted at CIRIMAT laboratory, with a new pure alumina grit, while the TBC systems were grit blasted at Snecma, using partially recycled alumina grit. Thus, the surface of the bond-coating could have been polluted before thermal barrier deposition which would lead to higher oxidation rates and thicker TGO. Finally, the very slow heating performed to reach the oxidation temperature of 1100 °C, which was equal to 5 °C/min, could also be responsible for the difference in TGO thickness observed with and without the TBC (the heating rate for the “superalloy + bond-coating” systems was equal to 60 °C/min).

Such a difference in TGO thickness with and without the TBC has already been observed by Tolpygo and Clarke with non-grit blasted Pt-modified nickel aluminide bond-coating [9].

The comparison between the systems without a pre-oxidation and the systems with pre-oxidation under synthetic air highlights the effect of temperature on the first oxide that forms (Fig. 15). Even though the TGO layers were not characterised after the first hour of oxidation at 1100 °C (without a pre-oxidation step), the morphology at the surface of the TGO layer differed. Without a pre-oxidation, elongated grains were visible on top of the TGO whereas equiaxial grains appeared on top of the TGO after pre-oxidation and oxidation under air. The elongated grains were reminiscent of the morphology of transient alumina or transient oxides. Consequently, the same argument as that exposed in the previous paragraph can be put forward. If a thermal barrier is applied to the bond-coating and no pre-oxidation carried out, the presence of transient oxides could lead to the development of a mixed zone with YSZ and a thicker TGO. Knowing that the TBC system lifetime is strongly dependent on the TGO thickness it is important to control the first oxide that forms on the bond-coating surface, before the thermal barrier deposition.

Conclusions

The present work dealt with the effects of Pt addition and of pre-oxidation on the oxidation behaviour of a NiCoCrAlYTa bond-coating made by the “Tribomet” process. First, it was shown that selective oxidation of aluminium was enhanced by platinum addition. Because the formation of fast growing oxides was prevented, the oxidation rate decreased and the adherence of the TGO layer increased. Even with the addition of Pt, the superalloy composition influenced the oxidation kinetics of the systems. More specifically, the presence of a reactive element within the

superalloy resulted in a decrease in the oxidation rate of Pt-modified NiCoCrAlYTa-base systems.

Another interesting point which needs further work was brought to light in this study. It concerns the possible effects of Pt on the stability of tantalum carbides. Above a critical concentration, Pt could cause the (Ta,Ti)C carbide precipitates to dissolve and then the release of the trapped titanium. Once the tantalum carbides are dissolved, titanium is free to diffuse from the superalloy towards the TGO. In the present study, titanium oxide did not lead to TGO spallation but the oxidation time was short and the amount of titanium oxide was low.

Pt did not seem to favour transient alumina formation for the coating composition and heating rate studied, but its effect on the first oxide that formed could be mitigated by the high Cr concentration within the bond-coating sub-surface. To favour the formation of a continuous α -Al₂O₃ layer before the deposition of the thermal barrier, a pre-oxidation step is necessary. Grit blasting removes the oxides that form during the diffusion heat treatment and makes the bond-coating surface uniform, which facilitates the formation of a protective exclusive alumina scale of uniform thickness and roughness. In our study, it was shown that a low oxygen partial pressure was required during pre-oxidation to favour the growth of α -Al₂O₃ relatively to the other oxides. Nevertheless, the oxidation temperature and duration need to be high enough in order to allow the formation of a relatively thick and protective α -Al₂O₃ layer.

Acknowledgments Turbomeca (Safran Group) are gratefully acknowledged for providing the samples and for the financial support of this study. Authors express their thanks to Praxair ST which manufactured the bond-coatings, to Snecma for grit blasting the TBC systems and to C.C.C which made EB-PVD thermal barrier coatings. J.P. Grenet from IPREM (Pau, France) is gratefully acknowledged for Raman and photoluminescence spectroscopy analyses, Turboméca and CNRS for the doctoral grant of A. Vande Put.

References

1. J. R. Nicholls, M. J. Deakin and D. S. Rickerby, *Wear* **233**, 352 (1999).
2. R. G. Wellman, M. J. Deakin and J. R. Nicholls, *Wear* **258**, 349 (2005).
3. C. Mercer, S. Faulhaber, A. G. Evans and R. Darolia, *Acta Materialia* **53**, 1029 (2005).
4. S. Krämer, S. Faulhaber, M. Chambers, D. R. Clarke, C. G. Levi, J. W. Hutchinson and A. G. Evans, *Materials Science and Engineering: A* **490**, 26 (2008).
5. A. G. Evans, D. R. Mumm, J. W. Hutchinson, G. H. Meier and F. S. Pettit, *Progress in Materials Science* **46**, 505 (2001).
6. D. Strauss, G. Müller, G. Schumacher, V. Engelko, W. Stamm, D. Clemens and W. J. Quadackers, *Surface & Coatings Technology* **135**, 196 (2001).
7. D. Monceau, F. Crabos, A. Malie, B. Pieraggi, *Materials Science Forum*, **369–372**, 670 (2001).
8. H. Lau, C. Leyens, U. Schulz and C. Friedrich, *Surface & Coatings Technology* **165**, 217 (2003).
9. V. K. Tolpygo and D. R. Clarke, *Surface & Coatings Technology* **200**, 1276 (2005).
10. B. Baufeld and U. Schulz, *Surface & Coatings Technology* **201**, 2667 (2006).
11. M. Matsumoto, T. Kato, K. Hayakawa, N. Yamaguchi, S. Kitaoka and H. Matsubara, *Surface & Coatings Technology* **202**, 2743 (2008).
12. R. Mevrel, *Materials Science and Engineering* **A120**, 13 (1989).
13. J. R. Nicholls, *Jom-Journal of the Minerals Metals & Materials Society* **52**, 28 (2000).
14. J. R. Nicholls, *MRS Bulletin* Sept, 659 (2003).

-
15. D. P. Whittle and J. Stringer, *Philosophical Transactions of the Royal Society of London* **A295**, 309 (1980).
 16. G. Fisher, P. K. Datta, J. S. Burnell-Gray, W. Y. Chan and J. C. Soares, *Surface & Coatings Technology* **110**, 24 (1998).
 17. J. Toscano, R. Vaßen, A. Gil, M. Subanovic, D. Naumenko, L. Singheiser and W. J. Quadackers, *Surface & Coatings Technology* **201**, 3906 (2006).
 18. H. Guo, L. Sun, H. Li and S. Gong, *Thin Solid Films* **516**, 5732 (2008).
 19. E. J. Felten, *Oxidation of Metals* **10**, 23 (1976).
 20. R. Lowrie and D. H. Boone, *Thin Solid Films* **45**, 491 (1977).
 21. L. Peichl and D. F. Bettridge, Overlay and diffusion coatings for aero gas turbines, in *Materials for Advanced Power Engineering, Part I, Proceeding International Conference 1994, Liege* eds. D. Coutsouradis et al. (Kluwer Acad. Publ., Dordrecht, 1994), p. 717.
 22. T. A. Taylor and D. F. Bettridge, *Surface & Coatings Technology* **86–87**, 9 (1996).
 23. W. J. Quadackers, V. Shemet, D. Sebold, R. Anton, E. Wessel and L. Singheiser, *Surface & Coatings Technology* **199**, 77 (2005).
 24. N. M. Yanar, F. S. Pettit and G. H. Meier, *Metallurgical and Materials Transactions A* **37A**, 1563 (2007).
 25. A. Feuerstein, J. Knapp, T. Taylor, A. Ashary, A. Bolcavage and N. Hitchman, *Journal of Thermal Spray Technology* **17**, 199 (2008).
 26. F. H. Stott, B. Gleeson and P. Castello, *Materials at High Temperature* **16**, 15 (1999).
 27. X. Zhao, T. Hashimoto and P. Xiao, *Scripta Materialia* **55**, 1051 (2006).
 28. A. Vande Put, M.-C. Lafont, D. Oquab, A. Raffaitin, and D. Monceau, *Surface & Coatings Technology*, **205**, 717 (2010)
 29. V. K. Tolpygo, D. R. Clarke and K. S. Murphy, *Metallurgical and Materials Transactions A* **32A**, 1467 (2001).
 30. Web site <http://rruff.info/>. Accessed 6 Mar 2011.
 31. Web site http://riodb.ibase.aist.go.jp/rasmin/E_index.htm. Accessed 6 Mar 2011.
 32. R. Mevrel and C. Duret, in *Advanced Workshop: Coatings for Heat Engines*, Aquafredda di Maretea, Italy (1984).
 33. A. M. Huntz, A. Boumaza and G. Moulin, *Oxidation of Metals* **30**, 141 (1988).
 34. A. Boudot, PhD, National Polytechnic Institute of Toulouse, Toulouse, France (2000).
 35. S. Dryepondt, PhD, National Polytechnic Institute of Toulouse, Toulouse, France (2004).
 36. A. Raffaitin, PhD, National Polytechnic Institute of Toulouse, Toulouse, France (2007).
 37. B. Gleeson, W. Wang, S. Hayashi and D. Sordelet, *Material Science Forum* **461–464**, 213 (2004).
 38. E. Copland, *Thermodynamic Effect of Platinum Addition to beta-NiAl: An Initial Investigation*. Technical Report No. NASA/CR-2005-213330 (NASA, 2005).
 39. E. Copland, *Journal of Phase Equilibria and Diffusion* **28**, 38 (2007).
 40. D. Monceau and B. Pieraggi, *Oxidation of Metals* **50**, 477 (1998).
 41. Y. Cadoret, D. Monceau, M. Bacos, P. Josso, V. Maurice and P. Marcus, *Oxidation of Metals* **64**, 185 (2005).
 42. M. W. Brumm and H. J. Grabke, *Corrosion Science* **33**, 1677 (1992).
 43. D. Oquab, D. Monceau, Y. Thébault and C. Estournes, *Materials Science Forum* **595–598**, 143 (2008).
 44. J. L. Smialek, *Journal of the Minerals* **58**, 29 (2006).
 45. V. Déneux, Y. Cadoret, S. Hervier and D. Monceau, *Oxidation of Metals* **73**, 83 (2010).
 46. S. Chevalier, *Traitement de surface et nouveaux matériaux: Quelles solutions pour lutter contre la dégradation des matériaux à haute température* (Laballery Impr., University editions of Dijon, 2007), p. 164.
 47. B. A. Pint, *Oxidation of Metals* **45**, 1 (1996).
 48. U. Schulz, K. Fritscher and A. Ebach-Stahl, *Surface and Coatings Technology* **203**, 449 (2008).
 49. B. A. Pint, *Special Issue on Science & Technology of Alumina of the Journal of the American Ceramic Society* **86**, 686 (2003).
 50. B. A. Pint, K. L. More and I. G. Wright, *Materials at High Temperatures* **20**, 375 (2003).
 51. H. M. Tawancy, A. I. Mohamed, N. M. Abbas, R. E. Jones and D. S. Rickerby, *Journal of Materials Science* **38**, 3797 (2003).
 52. A. Hesnawi, H. Li., Z. Zhou, S. Gong and H. Xu, *Vacuum* **81**, 947 (2007).
 53. N. Vialas and D. Monceau, *Oxidation of Metals* **66**, 155 (2006).
 54. A. R. Nicoll and G. Wahl, Paper Presented at the “Superalloys 1984” (TMS, 1984), p. 805.

-
55. H. Nickel, D. Clemens, W. J. Quadackers and L. Singheiser, *Journal of Pressure Vessel Technology, Transactions of the ASME* **121**, 384 (1999).
 56. J. M. N. G. Muamba and R. Streiff, *Materials Science and Engineering* **A121**, 391 (1989).
 57. H. M. Tawancy, N. Sridhar and N. M. Abbas, *Journal of Materials Science* **35**, 3615 (2000).
 58. B. A. Pint, J. A. Haynes, K. L. More, I. G. Wright, and C. Leyens, Paper Presented at the Superalloys 2000 (TMS, Warrendale, PA 2000).
 59. A. M. Huntz, A. Boumaza, G. Moulin, and J. L. Lebrun, Paper Presented at the Advanced Materials and Processing Techniques for Structural Applications, Paris, France (1987).
 60. P. Fox and G. J. Tatlock, *Materials Science and Technology* **5**, 816 (1989).
 61. S. K. Bose and H. J. Grabke, *Zeitschrift fur Metallkunde* **69**, 8 (1978).
 62. M. W. Chen, M. L. Glynn, R. T. Ott, T. C. Hufnagel and K. J. Hemker, *Acta Materialia* **51**, 4279 (2003).
 63. M. W. Chen, R. T. Ott, T. C. Hufnagel, P. K. Wright and K. J. Hemker, *Surface and Coatings Technology* **163–164**, 25 (2003).
 64. D. S. Balint and J. W. Hutchinson, *Journal of the Mechanics and Physics of Solids* **53**, 949 (2005).
 65. V. K. Tolpygo and D. R. Clarke, *Acta Materialia* **48**, 3283 (2000).
 66. A. Vande Put, D. Oquab and D. Monceau, *Materials Science Forum* **595–598**, 213 (2008).
 67. J. A. Haynes, M. J. Lance, B. A. Pint and I. G. Wright, *Surface and Coatings Technology* **146–147**, 140 (2001).
 68. S. Laxman, B. Franke, B. W. Kempshall, Y. H. Sohn, L. A. Giannuzzi and K. S. Murphy, *Surface & Coatings Technology* **177–178**, 121 (2004).
 69. M. J. Stiger, N. M. Yanar, R. W. Jackson, S. J. Laney, F. S. Pettit, G. H. Meier, A. S. Gandhi and C. G. Levi, *Metallurgical and Materials Transactions A* **38A**, 848 (2007).
 70. U. Schulz, M. Menzebach, C. Leyens and Y. Q. Yang, *Surface & Coatings Technology* **146–147**, 117 (2001).
 71. K. S. Murphy, K. L. More and M. J. Lance, *Surface and Coatings Technology* **146–147**, 152 (2001).
 72. C. G. Levi, E. Sommer, S. G. Terry, A. Catanoiu and M. Rhüle, *Journal of the American Ceramic Society* **86**, 676 (2003).
 73. M. Hu, S. Guo, T. Tomimatsu, Y. Ikuhara and Y. Kagawa, *Surface & Coatings Technology* **200**, 6130 (2006).
 74. M. J. Stiger, N. M. Yanar, F. S. Pettit, and G. H. Meier, *Elevated Temperature Coatings: Science and Technology III* (The Minerals, Metals and Materials Society, Warrendale, PA, 1999), p. 51.
 75. H. Hindam and D. P. Whittle, *Oxidation of Metals* **18**, 245 (1982).